Science of the Total Environment 882 (2023) 163649

Contents lists available at ScienceDirect

Science of the Total Environment

journal homepage: www.elsevier.com/locate/scitotenv

As and S speciation in a submarine sulfide mine tailings deposit and its environmental significance: The study case of Portmán Bay (SE Spain)

A. Baza-Varas [b], J. Roqué-Rosell [a,*], M. Canals [b,*], J. Frigola [b], M. Cerdà-Domènech [b], A. Sanchez-Vidal [b], D. Amblàs [b], M. Campeny [c], C. Marini [d]

[a] Departament de Mineralogia, Petrologia i Geologia Aplicada, Facultat de Ciències de la Terra, Martí i Franquès s/n, 08028 Barcelona, Catalonia, Spain
[b] GRC Geociències Marines, Departament de Dinàmica de la Terra i de l'Oceà, Facultat de Ciències de la Terra, Martí i Franquès s/n, 08028 Barcelona, Catalonia, Spain
[c] Museu de Ciències Naturals de Barcelona, Passeig Picasso s/n, 08003 Barcelona, Catalonia, Spain
[d] CELLS – ALBA Synchrotron Radiation Facility, Carrer de la Llum 2-26, 08090, Cerdanyola del Vallès, Barcelona, Catalonia, Spain

HIGHLIGHTS

- As is affected by complex biogeochemical processes.
- Ore arsenopyrite is preserved and does not release As to the environment.
- Secondary scorodite releases As to the environment.
- Authigenic orpiment and realgar precipitate.
- SRB activity reduces and immobilizes As in the submarine mine tailings.

GRAPHICAL ABSTRACT

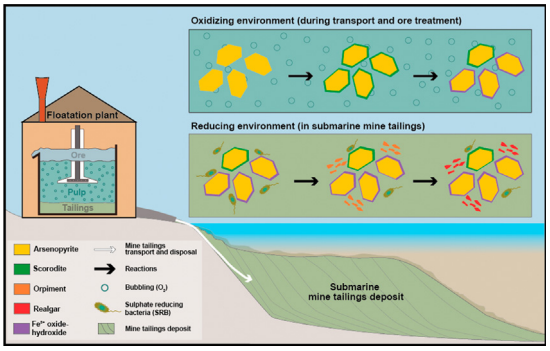

ARTICLE INFO

Editor: Jurgen Mahlknecht

Keywords:
Submarine mine tailings
Arsenic
Sulfur
Speciation
XAS
Environment

ABSTRACT

The dumping of an estimated amount of 57 million tons of hazardous sulfide mine waste from 1957 to 1990 into Portmán's Bay (SE Spain) caused one of the most severe cases of persistent anthropogenic impact in Europe's costal and marine environments. The resulting mine tailings deposit completely infilled Portmán's Bay and extended seawards on the continental shelf, bearing high levels of metals and As. The present work, where Synchrotron XAS, XRF core scanner and other data are combined, reveals the simultaneous presence of arsenopyrite (FeAsS), scorodite ($FeAsO_4{\cdot}2H_2O$), orpiment (As_2S_3) and realgar (AsS) in the submarine extension of the mine tailings deposit. In addition to arsenopyrite weathering and scorodite formation, the, the presence of realgar and orpiment is discussed, considering both potential sourcing from the exploited ores and in situ precipitation from a combination of inorganic and biologically mediated geochemical processes. Whereas the formation of scorodite relates to the oxidation of arsenopyrite, we hypothesize that the presence of orpiment and realgar is associated to scorodite dissolution and subsequent precipitation of these two minerals within the mine tailings deposit under moderately reducing conditions. The occurrence of organic debris and reduced organic sulfur compounds evidences the activity of sulfate-reducing bacteria (SRB) and provides a plausible explanation to the reactions leading to the formation of authigenic realgar and orpiment. The precipitation of these two minerals in the mine tailings, according to our hypothesis, has important consequences for As mobility since this process would reduce the release of As into the surrounding environment. Our work provides for the first time valuable hints on As speciation in a massive submarine sulfide mine tailings deposit, which is highly relevant for similar situations worldwide.

* Corresponding authors.
E-mail addresses: josep.roque@ub.edu (J. Roqué-Rosell), miquelcanals@ub.edu (M. Canals).

http://dx.doi.org/10.1016/j.scitotenv.2023.163649
Received 31 August 2022; Received in revised form 14 April 2023; Accepted 18 April 2023
Available online 23 April 2023

1. Introduction

Given that they are out of sight and because of the prevailing anoxic conditions, submarine environments have long been considered as good storing places for wastes from mining activities (Ramirez-llodra et al., 2022; Smedley and Kinniburgh, 2002). Tailings resulting from land mining of a variety of ores, including sulfides, have been dumped underwater in several coastal locations all over the world (Koski, 2012; Palau et al., 2021; Smedley and Kinniburgh, 2002). This has led to the release and accumulation in the marine environment of large amounts of metals and metalloids by the mining industry, which is in fact one of the main sources of this type of pollution globally (Domènech et al., 2002; Foster et al., 1998; Smedley and Kinniburgh, 2002). One such pollutants is arsenic (As), a naturally occurring metalloid widely found in the environment. As commonly exists in four oxidation states: As^{3-}, As^{0}, As^{3+} and As^{5+}. The less common native As^{0} occurs rarely in the environment whereas As^{3-} can appear in gases emanating from anoxic environments. Besides, As^{5+}, and aqueous $H_2AsO_4^-$ and $HAsO_4^{2-}$, are the predominant forms of inorganic As in aerobic environments. As^{3+}, in the aqueous forms H_3AsO_3 and $H_2AsO_3^-$, is more prevalent in anoxic environments and is more mobile and toxic (Smedley and Kinniburgh, 2002).

The ecotoxicological effects of As from underwater mine tailings, in all its naturally occurring forms, constitute a major concern despite of some reports stating that the reducing conditions in underwater environments should prevent the release of toxic elements (Shimmield et al., 2010; Vogt, 2013; Walder, 2015). However, a sound assessment of this issue requires a comprehensive understanding of the As biogeochemistry and the associated processes affecting the As-bearing minerals in the submarine mine tailings (García-lorenzo et al., 2014; Martínez-Gómez et al., 2012; Mestre et al., 2017). Portmán Bay (Murcia province, SE Spain) offers a unique opportunity to gain knowledge on the behavior of As within an easily accessible underwater coastal mine tailings deposit and to assess its potential environmental impact (Fig. 1). Such a study should also provide clues to anticipate some of the likely consequences of seabed mining, which is viewed as a future source of scarce metals for the energy transition and high-tech industries (Collins et al., 2013; Hughes et al., 2015; Simpson and Spadaro, 2016; Van Dover, 2011).

Prior research on the environmental hazards from the submarine mine tailings deposit of Portmán Bay is rather limited. Beyond some ecotoxicological studies (Auernheimer and Chinchon, 1997; Benedicto et al., 2011; Martínez-Gómez et al., 2012), there are a few recent publications providing insight on the role of groundwater discharge in remobilizing dissolved metals from the mine tailings pile into seawater, the subaquatic extension and distribution of the mine tailings, their composition, stratigraphy and depositional history (Alorda-Kleinglass et al., 2019; Baza-Varas et al., 2022; Cerdà-Domènech et al., 2019). More generally, and despite of its wide interest, the number of published studies quantifying As-bearing minerals and their behavior in underwater mine tailings also is quite scant, and mostly focuses in laboratory experiments and model simulations (Embile et al., 2018; Palau et al., 2021). These studies make assumptions on the mineralogy, the geochemistry and the As species occurring in the submarine mine tailings, which hinder the complexity behind the processes involved in As biogeochemistry (Cullen and Reimer, 1989; Palau et al., 2021; Smith et al., 2005). Various reasons can make advancing in the knowledge of the behavior of this metalloid particularly challenging, such as, the intricacy of given sedimentological settings, accessing and sample handling difficulties, and As occurrence in multiple phases, not to mention preventions for the results of some studies to see the public light (Alorda-

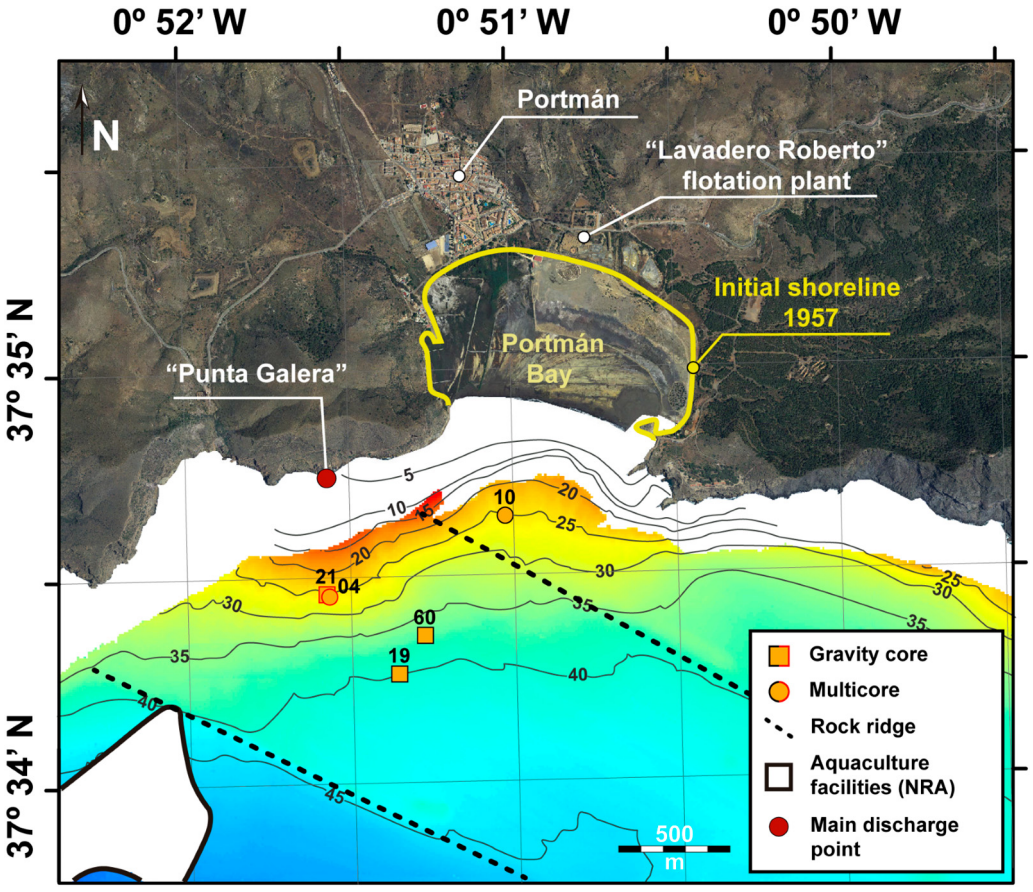

Fig. 1. Detailed map of the study area showing the location of the sediment cores used in this research. The yellow line corresponds to the coastline before the onset of en masse dumping of mine tailings, and the red point to the main discharge point of the mine waste through a pipeline sourced at the onshore floatation plant during 1997–1990 period. Depth contours are in meters. Land image is from 2011 and was obtained by the Spanish *Plan Nacional de Ortofotografía Aérea* (PNOA).

Kleinglass et al., 2019; Baza-Varas et al., 2022; Manteca et al., 2014; Wang et al., 2013).

Besides, the biogeochemical cycle of S in marine deposits may lead to important chemical and physical changes in As. In seabed sediments, the reduction of sulfate to sulfide is one of the most important terminal pathways of organic matter mineralization, driven by the oxidation of organic matter by sulfate reducing bacteria (SRB) using a wide range of metals and metalloids —i.e. Fe, Zn and As— as terminal electron acceptors (Alam and McPhedran, 2019; Jørgensen, 2021; Jørgensen et al., 2019; Le Pape et al., 2017; Moore et al., 1988). The SRB use organic molecules and H_2 to reduce sulfate to sulfide (H_2S), which is gradually oxidized in the sediments back to sulfate through a set of intermediate species —i.e. elemental sulfur (S^0), thiosulfate ($S_2O_3^{2-}$) and sulfite (SO_3^{2-}) (Jørgensen, 2021). During this process, sulfide reacts to form sulfide minerals that precipitate and get buried into the marine deposits, as illustrated by the formation of authigenic pyrite (FeS_2) (Jørgensen, 2021; Moore et al., 1988; Schoonen, 2004). Thus, the precipitation of authigenic sulfide minerals can likewise turn into an important sink for trace metals, with significant implications for the environmental fate of As (Farquhar et al., 2002; Huerta-Diaz and Morse, 1992; Le Pape et al., 2017). Furthermore, As toxicity also depends on its speciation, which can be impinged by biogeochemical processes in submarine sediments involving S (Gbaruko et al., 2008; Neff, 1997; Nesbitt et al., 1995). Therefore, a detailed analysis of submarine sulfide mine tailings focused on As-bearing minerals and As biogeochemistry is required (Baza-Varas et al., 2022; Cerdà-Domènech et al., 2019; Cullen and Reimer, 1989; Smedley and Kinniburgh, 2002).

Hence, evaluating the potential environmental impact of As in Portman's Bay requires identifying the As-bearing minerals and understanding their geochemistry and the complex biogeochemical interactions taking place in the submarine mine tailings (Kalia and Khambholja, 2015; Kerr et al., 2018; Neff, 1997; Oremland and Stolz, 2003). Accordingly, the ultimate goals of this study are: (i) to determine As and S speciation in the submerged sulfide mine tailings; (ii) to identify the physical, chemical and biological processes able to affect As mobility and toxicity; and (iii) to propose a methodology that could guide future studies on As biogeochemistry in submarine mine tailings deposits elsewhere (Hudson-Edwards, 2016; Koski, 2012).

2. Study area

In 1957, the mining company *Sociedad Minero Metalúrgica Peñarroya España* (SMMPE) opened a floatation concentration plant at short distance from the shoreline in Portmán Bay, to treat complex sulfide ores from Sierra Minera de Cartagena. During the plant's lifetime about 57 Mt. of tailings were dumped into the sea from 1957 to 1990, resulting in the complete infill of the bay, now occupied by hazardous artificial soils, and in a seaward shoreline shift of about 600 m (Baza-Varas et al., 2022; Frigola et al., 2017; Manteca et al., 2014; Oyarzun et al., 2013). Near 14 Mt. tailings from Sierra Minera de Cartagena's open mining pits, roughly equivalent to 5.6 Mm^3, have been estimated to form the bay's infill, which implies that a much larger volume lies on the adjacent seabed off Portmán Bay (Fig. 1) (Manteca et al., 2014). The treatment of the sulfide ores consisted of their blasting, crushing and milling to then separate the minerals physically in the floatation plant after their density and ability to adhere to air bubbles. The ore particles were thus carried to the surface, from where they were removed. The gangue staying in the liquid phase ended up forming the mine tailings (Manteca et al., 2014; Oyarzun et al., 2013). The volume of mine tailings represents >95 % of the initial mineralized rock, and still contained significant amounts of pyrite (FeS_2) and lesser amounts of galena (PbS), sphalerite (ZnS), arsenopyrite (FeAsS), silicates, oxides, and carbonates. Since no strict environmental regulations existed at that time, the mine tailings were disposed directly into the sea by means of a 2 km-long pipeline opening on a low coastal cliff to the west of the bay, in a place named Punta Galera (Fig. 1) (Baza-Varas et al., 2022; Frigola et al., 2017).

The submarine extension of the mine tailings deposit covers the seafloor down to 50 m of water depth on the inner part of a narrow (i.e. 11 km of width), southwards dipping continental shelf with its edge at about 110 m depth (Acosta et al., 2013) (Fig. 1). The broader study area is dominated by semi-arid conditions, this leads to the absence of permanent water courses opening into the sea (https://es.climate-data.org/europe/espana/regionde-murcia/cartagena-3213/). Accordingly, natural sediment inputs from inland are particularly scarce during most the time. The only exception occurs at the occasion of strong rainfall episodes leading to short-lived discharge events of the local *ramblas* or wadis. In pre-dumping times, such setting resulted in high water transparency easing the development of extensive seagrass meadows down to 40–45 m of water depth (Ruiz et al., 2015a). The massive dumping of sulfide mine tailings led to a sharp increase of sedimentation rates, to the suffocation of benthic habitats and to a severe environmental degradation of the entire area. The common finding of vegetal fibers and shell fragments in the lowermost levels of sediment cores reaching the base of the tailings deposit perfectly testifies the environmental disaster that took place there (Baza-Varas et al., 2022).

Such a massive dumping also modified dramatically the bathymetry off Portmán Bay's, which now shows a terrace adjacent to the coast down to 5–10 m of depth, depending on the specific location, followed by a steeper slope down to about 35 m that smoothens progressively towards the deeper reaches. Finally, an almost horizontal foot-of-slope area continues down to 50 m and beyond (Baza-Varas et al., 2022). This landscape is interrupted by a couple of parallel, NW-SE oriented, 3–4 m in height rocky ridges, which are clearly visible on the lower slope and foot-of-slope area described above, i.e. where not buried by the tailings. The mine tailings themselves form a coastal prograding sedimentary body with a topset (the very shallow coastal terrace), a foreset (the slope) and a bottomset (the foot-of-slope) (Baza-Varas et al., 2022). Overall, the submarine mine tailings are estimated to extend about 3 and 2 km in the *E*-W and N-S directions, respectively (unpublished data). From bottom to top four main sedimentary units have been identified to form the submarine mine tailings (Baza-Varas et al., 2022). Unit 1 corresponds to natural sediments constituting the original seabed before the dumping of mine tailings. Unit 2 represents the initial stage of mine tailings accumulation, i.e. the transition from natural sedimentation to the massive accumulation of sulfide mine tailings. Unit 3 encompasses the bulk of mine tailings and is made of several interbedded facies. Finally, Unit 4 depicts the transition from mine tailings accumulation to a new stage of "natural" sedimentation, i.e. a mix of reworked and newly accumulated materials following the cessation of dumping (Baza-Varas et al., 2022; Manteca et al., 2014; Oyarzun et al., 2013). According to its scope, the present study focuses in Unit 3 and also considers Unit 4 (Fig. 2).

3. Materials and methods

3.1. Sampling of the submarine mine tailings

Two research cruises, NUREIEV-3 (23rd – 29th April 2016) and NUREIEVA-MAR1 (27th June to 10th July 2018) onboard the Spanish research vessel "Ángeles Alvariño", from the Spanish Institute of Oceanography (IEO), allowed obtaining a number of sediment cores (Baza-Varas et al., 2022; Cerdà-Domènech et al., 2019) of which a selection has been used to study As and S speciation in Portmán's Bay submarine mine tailings deposit (Fig. 1). Short sediment cores from the very top layers were obtained by means of a KC Denmark multicorer (MC) while long sediment cores from the bulk of the submarine mine tailings deposit were obtained using a 5 m long gravity corer (GC) see (Baza-Varas et al., 2022; Cerdà-Domènech et al., 2019) for details. The two types of sediment cores, MC and GC, were distributed to sample the most representative units forming the tailings deposit, as identified from very high resolution multibeam bathymetry and topographic parametric seismic reflection data (not described here).

Two of the MCs —MC04 and MC10— were selected for this study, which were collected at rather short distance from the shoreline (Fig. 1), in the upper layers of the clinoform formed by the coastal mine tailings deposit. Three of the GCs were also selected, which were GC21 —collected at

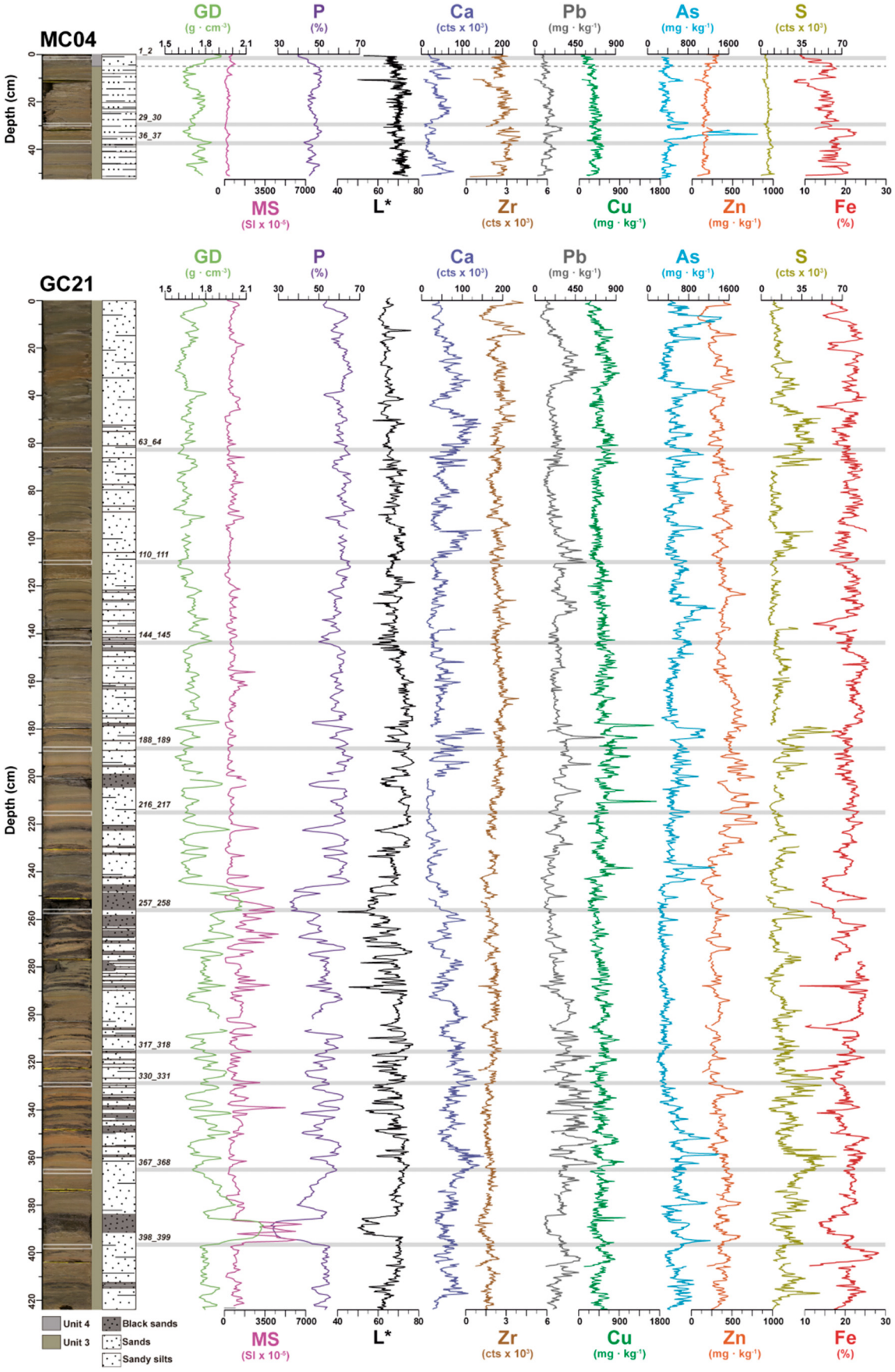
MC04
GC21
Depth (cm)
GD (g · cm⁻³)
P (%)
Ca (cts x 10³)
Pb (mg · kg⁻¹)
As (mg · kg⁻¹)
S (cts x 10³)
MS (SI x 10⁻⁵)
L*
Zr (cts x 10³)
Cu (mg · kg⁻¹)
Zn (mg · kg⁻¹)
Fe (%)
1_2
29_30
36_37
63_64
110_111
144_145
188_189
216_217
257_258
317_318
330_331
367_368
398_399
Unit 4
Unit 3
Black sands
Sands
Sandy silts

about the same location than MC04—, and GC19 and GC60, all obtained from the lower foreset or frontal slope of the submarine mine tailings clinoform, i.e. at larger distance from the main discharge point than the previous cores (Fig. 1). Cores MC04, GC19, GC60 and GC21 are located in the central part of the mine tailings deposit, in-between the two rocky ridges mentioned above (Fig. 1). The cores' metadata and description details are provided in the Supplementary section. To ensure their preservation following recovery, all cores were kept in PVC liners and stored at 4–5 °C both while onboard and during their transfer to University of Barcelona (UB) and ALBA Synchrotron premises. Materials within the core liners were maintained intact to first perform continuous non-destructive Multi Sensor Core Logger (MSCL) analyses. Then they were split in two halves to follow on with XRF scanning continuous non-destructive analyses. Finally, selected sections were subsampled under controlled conditions for further geochemical characterization in the geochemistry lab and in the synchrotron.

3.2. Non-destructive analysis of sediment cores

A range of continuous, non-destructive analyses were performed at UB's CORELAB facility to determine the internal structure, the physical properties and the chemical composition of GC21 and MC04 cores by means of a Geotek MSCL and an Avaatech X-ray fluorescence (XRF) core scanner (XRF). MSCL data were acquired on intact (i.e. not opened) core sections to record gamma density (GD) and magnetic susceptibility (MS) with a 5 mm lineal resolution. GD was acquired using a Cs^{137} capsule as gamma ray source, emitting at 0.0662 MeV and collimated through a 5 mm slit. MS was measured my means of a Bartington point sensor (MS2E) producing a low intensity and non-saturating, alternating magnetic field at 2 kHz. Sediment porosity was subsequently calculated assuming a quartz density of 2.65 g cm^{-3} for the mineral component of the materials. Afterwards, the core sections were split, visually inspected, and imaged using a high-resolution color line scan camera mounted on the XRF core scanner with a 70 μm lineal resolution. Then, XRF profiles were obtained with a 2 mm lineal resolution on the split core sections, to semi-quantitatively determine compositional variations while paying special attention to the distribution of metals and As in the stratigraphic units formerly defined by (Baza-Varas et al., 2022). During XRF measurements, the excitation conditions were set at low energies at 10 kV and 1.0 mA without filter and 10 s dwell time, and at high energies at 30 kV and 1.5 mA using a Pd filter and 50s dwell time. Several metals (Ca, Zr, Pb, Zn, Cu and Fe), metalloids (As) and non-metallic (S) elements were selected as proxies for geogenic and anthropogenic influences, and some of them, namely Pb, Zn, Cu, Fe and As, were calibrated according to (Cerdà-Domènech et al., 2019).

3.3. Powder X-ray diffraction of materials

To probe the presence of As-bearing minerals, the mineral phases in the collected cores were identified and quantified by means of powder X-Ray diffraction (XRD). For that purpose, 2 samples were scooped from the central part of GC19 (sample GC19_19_20 cm, belonging to stratigraphic Unit 4) and GC60 (sample GC60_15_16 cm from stratigraphic Unit 3). These subsamples were manually disaggregated and grinded down to <5 μm with a pestle in an agata mortar. The resulting powder was placed on a non-oriented smear slide and analyzed using a PANalytical X'Pert PRO MPD Alpha1 diffractometer in Bragg-Brentano θ/2θ geometry applying nickel filtered Cu Kα radiation (1.5418 Å) at 45 kV and 40 mA with a X'Celerator detector at the Scientific and Technological Centres of University of Barcelona (CCiTUB). The powder XRD patterns were acquired from 4 to 80° 2θ scans with a step size of 0.017° and 80 s dwell time. The mineral phases were identified and quantified using the X'Pert Highscore software. It is to be noted that the high Fe contents in the cored materials hindered identifying the presence of minerals at low concentrations (2–5 % wt).

3.4. Scanning electron microscopy of materials

The mineral chemistry of the materials was determined by means of Scanning Electron Microscopy (SEM) coupled with Energy Dispersive X-ray Spectroscopy (EDS) and Backscattering Electron Imaging (BSE) with an Oxford Instruments INCA EDS detector, at 20 kV and 60 s dwell time at CCiTUB. The two subsamples selected for such analyses were scooped from the central part of MC10 core (samples MC10_7_8 cm and 10_11 cm, belonging to stratigraphic units 4 and 3, respectively), embedded in epoxy resin, polished, and covered with carbon using an Emitech K-950 × (9×10^5 Pa) high-vacuum evaporator at CCiTUB.

3.5. Synchrotron X-ray absorption analysis

The selected core sections were subsampled at ALBA Synchrotron facilities while taking into account their likely representativeness of the whole mine tailings submarine deposit. Special attention was given to the anthropogenic (i.e. the tailings) and the post tailings materials to better asses the transformation of sulfides within Portmán's Bay deposit. Subsampling tried to cover the maximum possible length of materials while preventing sample contamination by scooping every 30–60 cm from the central part of cores MC04 and GC21. Analyses were made by means of synchrotron X-ray absorption spectroscopy (XAS), namely using the X-ray absorption near-edge spectroscopy (XANES) technique, which provides a highly suitable approach to obtain detailed chemical and structural elemental data from materials with complex compositions (Mosselmans et al., 2008, 2009; Roqué-Rosell et al., 2017). In fact, because of this XANES has been rather widely used in studies on As and S in a variety of As-bearing systems, including underwater deposits (Foster et al., 1998; Hopp et al., 2008; Manceau et al., 2007; Marcus et al., 2004; Nicholas et al., 2017; Paktunc, 2013; Pfeifer et al., 2004; Vairavamurthy et al., 1994; Wang et al., 2013; Wilke et al., 2001). A set of natural crystalline minerals from the collection of the Museum of Natural Sciences of Barcelona were selected as As and S standards to calibrate the XANES spectra and determine As and S speciation. These were MCNB02 arsenopyrite (FeAsS), MCNB15 orpiment (As_2S_3), MCNB05 scorodite ($FeAsO_4{\cdot}2H_2O$), MCNB22 gypsum ($CaSO_4{\cdot}2H_2O$) and MCNB17 pyrite (FeS_2).

Measurements were carried out at the CLAESS beamline of the ALBA Synchrotron facility, which provides the required energy range (2.4–63.2 KeV) and a dedicated set up for handling air sensitive samples (Simonelli et al., 2016). To minimize sample exposition to air and prevent the oxidation of materials, we followed (Nicholas et al., 2017) approach, which consists of cutting and sealing into 20 cm sections the materials encased in PVC liners, transferring them to the synchrotron facility and placing them within a globe box under a N_2 controlled atmosphere. Afterwards, core sections were split and batches of material were scooped out from each section and set into specifically designed Teflon® cells. The cells were sealed using a 2.5 μm thick Mylar® film, let to stabilize within the globe box for 2–5 min, and then quickly transferred to the experimental hutch and placed in the vacuum chamber (Simonelli et al., 2016). Once the samples were in place, XANES scans up to 300 eV above the As and S K-edge absorption thresholds were acquired using a 50 μm aperture tungsten pinhole to reduce the photon flux and prevent beam damage while ensuring high quality XANES. During the experiments, the X-rays' beam path was maintained in vacuum to prevent absorption when working at low energies (Nicholas et al., 2017; Simonelli et al., 2016). The monochromator was calibrated in high energy using the Au L3-edge absorption at 11919.06 eV from an Au thin foil measured in transmission and calibrated in low energy using

Fig. 2. Color photograph, lithology, stratigraphy, and physical and chemical composition logs of MC04 (top) and GC21 (bottom) cores. Location data are provided in Table 1 and shown in Fig. 1. GD: gamma density; L*: color parameter; MS: magnetic susceptibility; P: porosity (calculated after Last and Smol, 2002). Ca, Zr and S concentrations are presented in counts (cts) while values for the rest of elements appear in mg kg^{-1} after Baza-Varas et al. (2022) calibration. Also note that Fe concentrations are expressed in percentage. Subsamples for synchrotron and other analyses are marked by thin horizontal grey stripes.

the S K-edge absorption at 2483.12 eV from a natural gypsum standard (S^{6+}) measured in fluorescence mode. The calibration in between the measurements was performed by checking the monochromator glitches, to ensure that all measurements sat on the same energy range.

Both the As and S K-edge XANES measurements on the selected samples were acquired in fluorescence mode using an Amp-Tek® silicon drift diode detector positioned at 90° from the incident beam. All experiments were conducted under vacuum, at room temperature and no photon induced oxidation was observed on the samples. Nevertheless, all As and S K-edge XANES data were collected in "quick" mode, performing a full energy scan in 30 s to minimize sample exposition to the X-rays. The overall number of energy scans per sample varied depending on the quality of the spectra. For most samples, 5 to 10 scans were enough, though a few diluted samples required >20 scans to completely resolve the spectra.

XANES data reduction (calibration, background subtraction and normalization) was performed using the ATHENA Package (Ravel and Newville, 2005). The As K-edge XANES data analysis was carried out by means of the Linear Combination Fitting (LCF) of ATHENA as well, subsequently representing the spectrum of each measured sample as a linear combination of a smaller number of component spectra from the selected mineral standards. To identify S compounds in the mine tailings in the absence of appropriate S standards, the S K-edge XANES data analysis was executed after the integrated cross section of each measured white line as in (Xia et al., 1998). To do so, the acquired S K-edge XANES were fitted using a series of Gaussian functions that represent s → p transitions, and arctangent step functions that represent the transitions of the ejected photoelectrons. Then, linear correlation was used to locate the energy positions of each Gaussian peak and identify the S oxidation states in the samples. In addition, the obtained Gaussian peak areas have also been utilized to estimate the percentage of total S in different oxidation states (Xia et al., 1998). Deconvolution of each S K-edge XANES spectra into pseudo components was accomplished by means of nonlinear least-square fittings, applying a dedicated code written in Python that employs basic modules and functions from the available libraries (Hunter, 2007; McKinney, 2010; van der Walt et al., 2011; Virtanen et al., 2020).

4. Results: characterization of the submarine mine tailings

4.1. Physical and chemical properties

Unit 3 materials consist of olive, orange and greyish clays, silts and fine to medium sands showing laminations, cross laminations, deformation structures and fining upwards sequences associated to grain size and color changes. The prevalence of fine sediments in Unit 3 is attributed to the crushing and grinding processes of the mineral ores prior to the dumping of the tailings into the sea (Oyarzun et al., 2013). Such a heterogeneous character of the mine tailings unit is well reflected in the variations of the materials' physical and chemical properties. For instance, the measured GD values are lower and more uniform in the upper part of the unit compared to the deeper part where they are higher and more fluctuating (i.e. below 250 cm in core GC21) (Fig. 2). Accordingly, the porosity curve shows an opposite pattern, with higher values (50–70 %) in the sandy silts of the upper part of the same core, and generally lower (30–50 %) and more oscillating values below 250 cm core depth where black sand layers are more common. Both GD and porosity shifts are well marked at the indicated core depth (Fig. 2). The measured MS in Unit 3 is rather uniform, with only some spikes of which the most prominent in the lower part of core GC21 are linked to the presence of black sands (Fig. 2). Color variations, as expressed by the L* parameter, display an alternation of lighter and darker levels with a tendency of the later to increase bottomwards (Fig. 2).

In terms of chemical composition, Unit 3 shows high contents of S and Fe, heavy metals such as Zn (76–976 mg kg^{-1}), Cu (89–1688 mg kg^{-1}) and Pb (53–765 mg kg^{-1}), and the metalloid As (160–1400 mg kg^{-1}). These element concentrations are rather variable along core GC21 with higher values of S, Pb and As occurring in its lowermost part. Besides, Ca (9–153 × 10^3 cts) and Zr (0.6–4 × 10^3 cts) show lower values in Unit 3 materials than those measured in natural sediments below the mine tailings deposit, which led (Baza-Varas et al., 2022) using them as geogenic proxies. Overall, the elemental composition of Unit 3 fits with the sulfide ore sourcing of the tailings. The topmost Unit 4 was not recovered in core GC21, likely because it was lost during coring. That is why we have considered core MC04, collected at the same location that GC21, which contains a few centimeters of Unit 4 (Fig. 1). Nonetheless, this unit —with a maximum thickness of a few tens of centimeters— has been extensively recovered in the study area, as shown for instance in the other cores included in the Supplementary section.

The materials forming the topmost Unit 4 consist of massive dark grey to black sandy silts and silts with fine sands presenting visible signs of bioturbation (Baza-Varas et al., 2022). In core MC04, the shift from Unit 3 to Unit 4 is marked by a noticeable increase in GD and a parallel drop in porosity (44–58 %). MS shows a slight increase, punctuated by a spike, with respect to the materials immediately below belonging to Unit 3 (Fig. 2). Unit 4 shows high contents of S and Fe (2.5–22.7 %), and also of heavy metals such as Zn (33–299 mg kg^{-1}), Cu (34–549 mg kg^{-1}), Pb (35–309 mg kg^{-1}) and the metalloid As (200–2235 mg kg^{-1}). As in bulk Unit 3 materials, Ca (9–80 × 10^3 cts) and Zr (0.5–4 × 10^3 cts) also presents lower values than natural sediments. Unit 4 represents the re-establishment of the natural sedimentary depositional rate, although the presence of pollutant proxies still is highly relevant (Baza-Varas et al., 2022).

4.2. Mineralogical composition

SEM images from Unit 4 samples show matrix-supported detrital sediments formed by clays and silts, and an abundant presence of sulfide minerals with a wide range of textures (Fig. 3). The predominant sulfide mineral is pyrite along with other ore minerals such as galena, sphalerite, and minor amounts of arsenopyrite. Most of the sulfides present subdimorphic to allotriomorphic habits, due to the mechanical crushing of the ores. Botryoidal and framboidal textures are also observed, which suggests dissolution and precipitation processes likely associated to microbial activity in the submarine mine tailings (Jørgensen et al., 2019; Smedley and Kinniburgh, 2002; Wang et al., 2020). Besides, SEM images also confirm the presence of abundant silicates (quartz, feldspar, muscovite and zircon), carbonates (calcite and siderite), oxides (magnetite, chromite and ilmenite) and possibly low crystallinity (oxyhydr)oxides that could be tentatively attributed to goethite as in (Manteca et al., 2014).

4.3. As and S speciation

The acquired As K-edge XANES obtained on the selected standards resulted in characteristic maximum intensity absorption peaks at 11868 eV for arsenopyrite (As^{1-}), at 11868.6 eV for realgar (As^{2+}), at 11868.9 eV for orpiment (As^{3+}) and at 11874.8 eV for scorodite (As^{5+}) (Fig. 4). The obtained As K-edge XANES absorption edges increased in height, decreased in width and shifted to higher energies with the increase of the As oxidation state. However, despite the calibration and associated precautions to ensure that all measurements were on the same energy range, we noticed some minor variations on the As K-edge XANES maximum intensity absorption positions when compared to values in the literature (Diacomanolis et al., 2016; O'Day et al., 2004; Wang et al., 2013). Such minor variations are thought to be related to the beamline's monochromator energy resolution and, possibly, to the presence of small amounts of As_2O_3 on some natural samples (Diacomanolis et al., 2016; O'Day et al., 2004; Simonelli et al., 2016). Even so, the measured As K-edge XANES spectra allowed determining the oxidation states of As in the submarine mine tailings using the standards as valence state references (Figs. 4). Besides, most of the acquired As K-edge XANES on the selected MC04 and GC21 samples present two characteristic absorption peaks: a low energy peak located between 11,868–11,869.9 eV, and a higher energy peak at 11874.8 eV, which indicate the presence of multiple As oxidation states in the investigated mine tailings (Figs. 4).

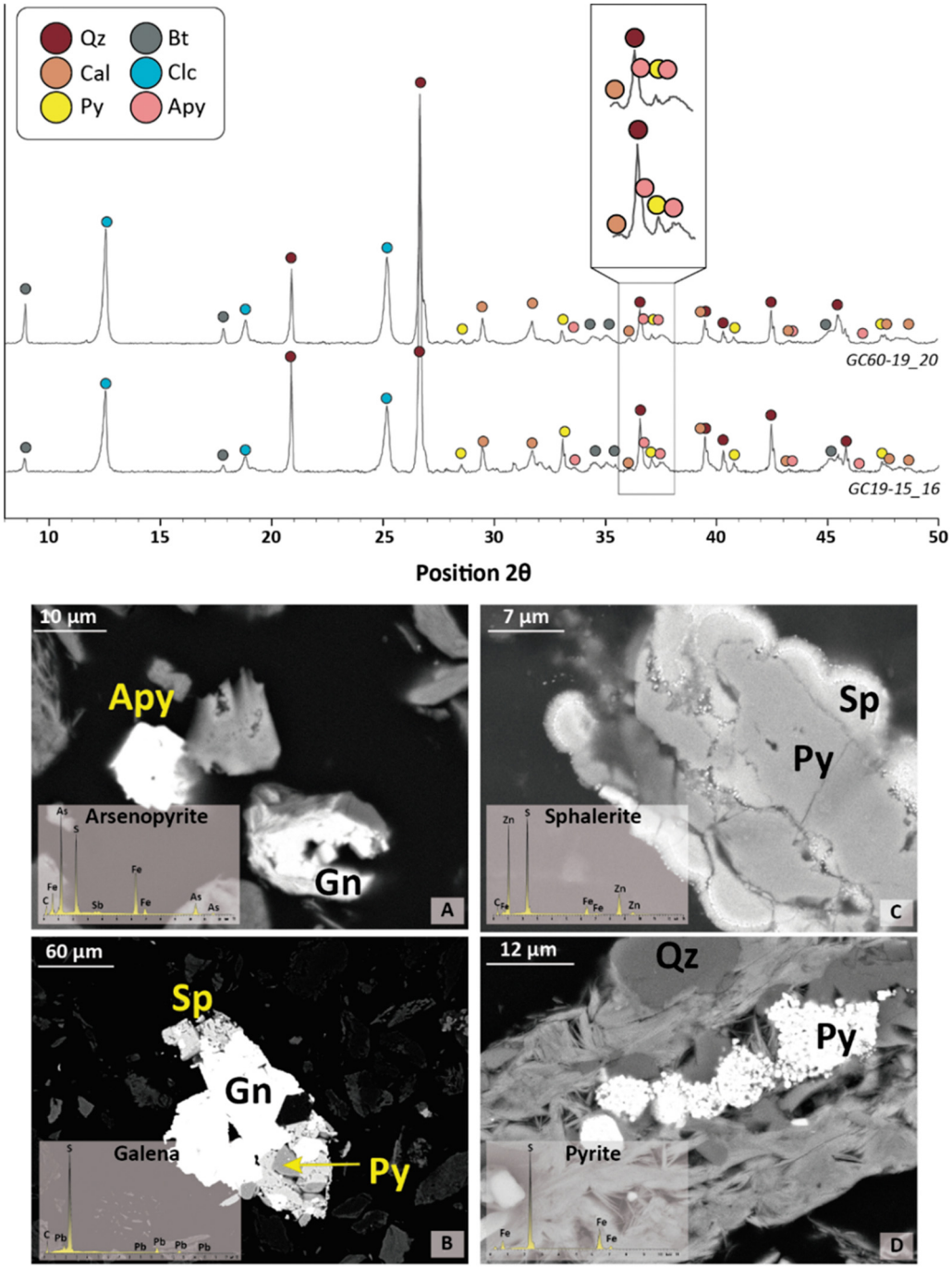

Fig. 3. X-Ray diffractograms (XRD), in 2θ scale, of two Unit 4 samples from GC19 and GC60 (cf. Table 1). Mineral phases are shown in 100 % intensity peaks, according to X'Pert HighScore patterns. SEM images are from MC10 (cf. Table 1). EDX analysis are presented for each mineral. A: Isolated ~120 µm grain with a pyrite, galena (triangular pit) and sphalerite association. B: Botryoidal sphalerite aggregate containing a pyrite grain. Some microspheres are observable in the outer and inner limits of sphalerite. C: Framboidal aggregates of densely packed pyrite microspheres deposited in fibrous silicates and quartz grains. D: Isolated arsenopyrite and galena grains of 10 and 15 µm. Apy: arsenopyrite; Bt: biotite; Cal: calcite; Clc: clinochlore; Gn: galena; Py: pyrite; Qz: quartz, Sp: sphalerite.

The As K-edge XANES spectra from MC04 samples display a broadening and shifting of the low energy absorption peak above 11,869 eV, just above arsenopyrite, from the uppermost part of Unit 3 (36_37 cm and 29_30 cm subsamples) to Unit 4 (1_2 cm subsample) (Fig. 2). Further, the observed As K-edge absorption shows a shift from 11,866.6 eV up to 11,866.8 eV, which is attributed to the simultaneous presence of As^{1-} and increasing amounts of As^{2+} and As^{3+} in the samples (Fig. 4). Accordingly, LCF data also demonstrate the presence and content variations of arsenopyrite and minor amounts of realgar and orpiment in both units (Figs. 5, 6 and Table 1). Besides, the higher energy absorption peak at 11874.8 eV experiences an increase in intensity from Unit 3 (36_37 cm and 29_30 cm) to Unit 4 (1_2 cm) due to an increase in As^{5+} contents (Fig. 4). Accordingly, the obtained LCF also shows an increase of scorodite from Unit 3 (36_37 cm and 29_30 cm) to Unit 4 (1_2 cm) and an associated decrease of arsenopyrite. The As K-edge XANES data thus confirm the simultaneous presence of arsenopyrite, scorodite, orpiment and realgar in MC04 core materials (Figs. 5, 6 and Table 1). Furthermore, the LCF data also display the arsenopyrite, scorodite, orpiment and realgar content variations associated to a decrease of As^{1-} and As^{2+} and an increase of A^{3+} and As^{5+} from the mine tailings *senso stricto* (i.e. uppermost part of Unit 3) to the mixed

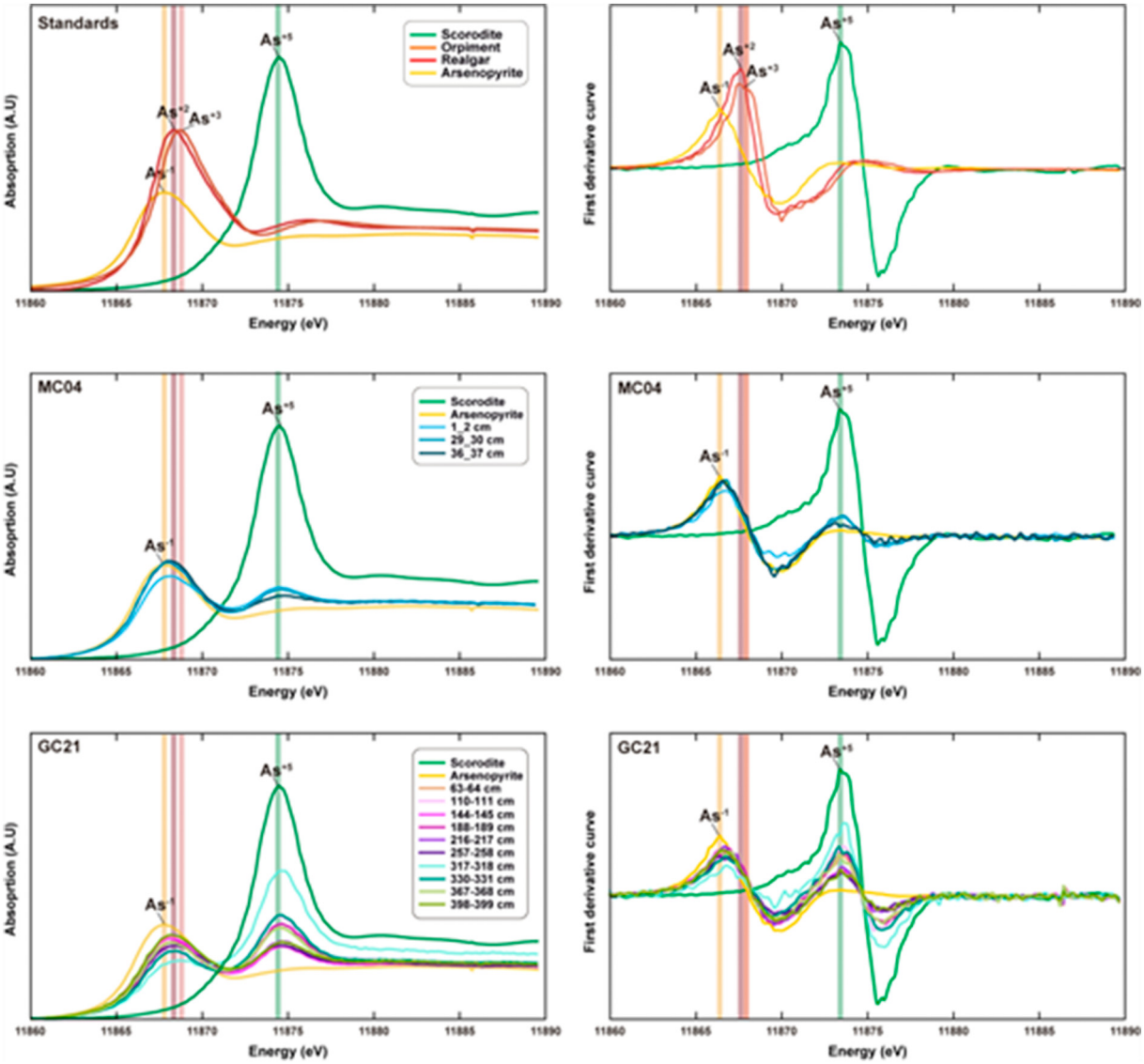

Fig. 4. On the left, As K-edge XANES spectra with the highlighted maximum absorption peaks from arsenopyrite (As^{1-}) at 11868 eV, realgar (As^{2+}) at 11868.6 eV, orpiment (As^{3+}) at 11868.9 eV and scorodite (As^{5+}) at 11874.8 eV. On the right, first derivative curve with the highlighted absorption As K-edge positions from arsenopyrite (As^{1-}) at 11866.5 eV, realgar (As^{2+}) at 11867.4 eV, orpiment (As^{3+}) at 11867.8 eV and scorodite (As^{5+}) at 11873.6 eV. The upper row corresponds to the standards, the intermediate to core MC04 samples, and the lower one to core GC21 samples. In GC21 samples both the first absorption intensity peak and the As K-edge are shifted towards higher energies, which are closer to realgar values. In addition, in GC21 samples the second absorption intensity peak increases significatively in Unit 3 when compared to Unit 3 and Unit 4 samples from core MC04, thus pointing to the presence of significant amounts of As^{5+}.

post-dumping materials on top (Figs. 5, 6 and Table 1). The observed increase of higher deviation LCF values from Unit 3 to Unit 4 relates to spectra differences within the lower energies and agrees with the presence of multiple As oxidation states in the materials (Figs. 5, 6 and Table 1).

The As K-edge XANES spectra from core GC21 samples also display a broadening and shifting of the low energy absorption peak above 11,869 eV and an associated As K-edge absorption shift, from 11,866.6 eV up to 11,866.9 eV, which is attributed to the simultaneous presence of As^{1-} and varying amounts of As^{2+} and As^{3+} (Fig. 4). Besides, the high energy absorption peak at 11874.8 eV experiences intensity variations due to significant changes in As^{5+} content, with maximum absorption intensity peaks in the lower Unit 3 (317_318 cm subsample, Fig. 2). This is further confirmed by our LCF data demonstrating the simultaneous presence of arsenopyrite, scorodite, orpiment and realgar associated to the presence of As^{1-} and As^{5+}, with minor amounts of As^{2+} and As^{3+} (Figs. 5, 6 and Table 1). While the distribution of arsenopyrite and scorodite is continuous along core GC21, the presence of realgar and orpiment is uneven, thus pointing to an ongoing set of processes affecting As speciation in the submarine mine tailings. Consequently, LCF data show an increase of scorodite and realgar at the expenses of arsenopyrite. Nevertheless, orpiment does not seem to follow the same pattern, as it increases towards the lower part of the core (Unit 3) where the overall porosity is lower than at the upper part (i.e. from 398_399 cm to 216_217 cm) (Figs. 2 and 4).

The S K-edge XANES from the selected samples shows three distinct maximum absorption peaks at 2472 eV, 2481.2 eV and 2483 eV (Fig. 7). Comparing the positions of these absorption peaks to those in reference compounds found in the literature (Solomon et al., 2011; Vairavamurthy et al., 1994; Xia et al., 1998) allows identifying a range of characteristic features: the absorption peak at 2470–2473.65 eV correspond to reduced organic and inorganic S compounds; the absorption peaks at 2480.4–2481.5 eV conform to less reduced organic compounds; and the absorption peak at 2482.5–2483.12 eV refer to oxidized S compounds (Fig. 7). By checking the available reference spectra eases the interpretation of most features in the S K-edge XANES from our samples. Subsequently, the first

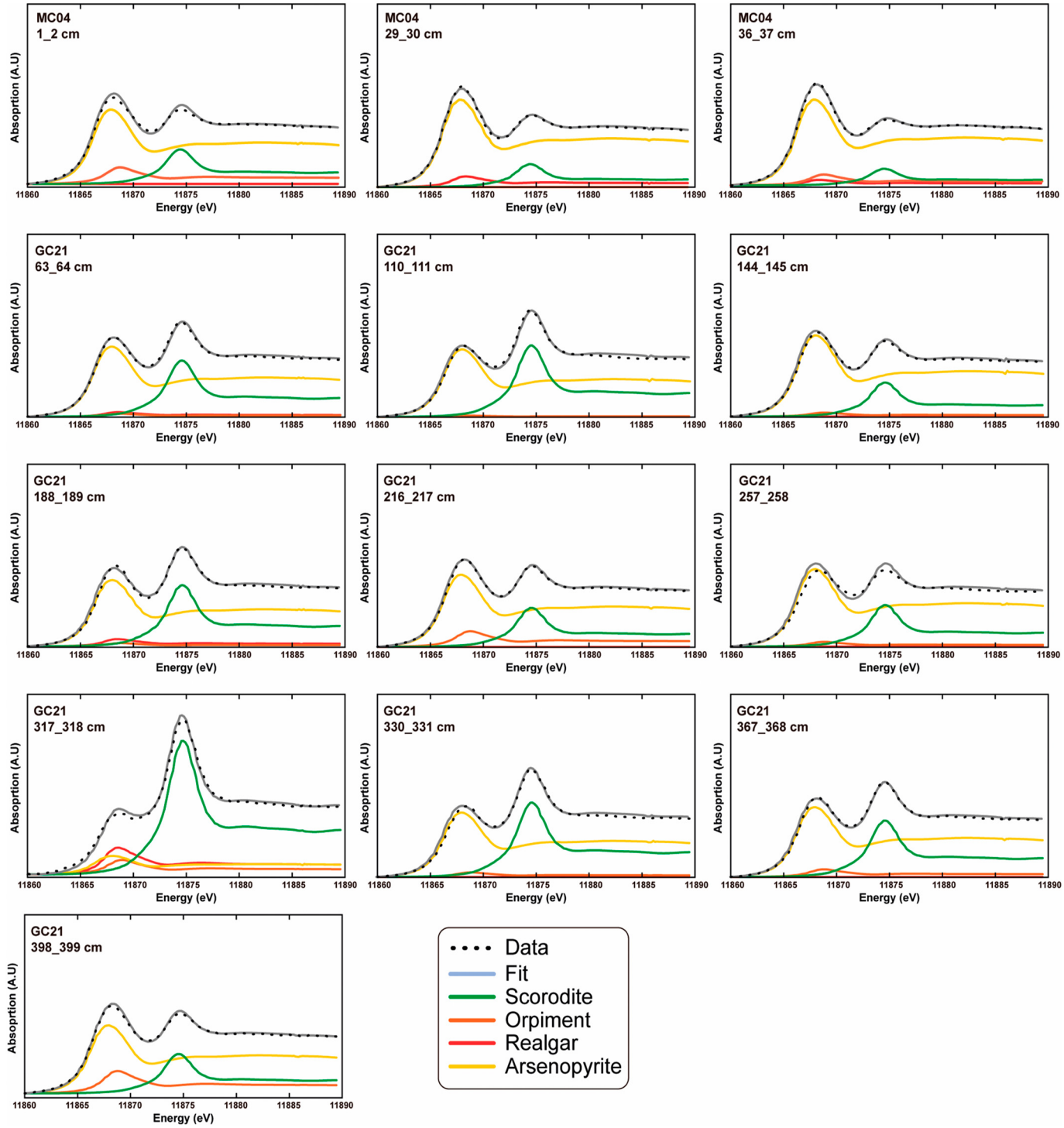

Fig. 5. As K-edge XANES data analysis are shown in three subsamples from MC04 and ten subsamples from GC21 core sediments. The results are obtained from fitting to the subsamples obtained spectra with a combination of arsenopyrite (FeAsS), realgar (AsS), orpiment (As_2S_3) and scorodite ($FeAsO_4{\cdot}2H_2O$) selected standards. The resulting As K-edge XANES R-factor LCF fitting values range from 3.71×10^{-4} to 8.7×10^{-3}. The As K-edge XANES data and LCF fit spectra confirm that arsenopyrite is the main As-bearing mineral in almost all subsamples, followed by scorodite and to a lesser extent realgar and orpiment. Besides, while the distribution of arsenopyrite and scorodite is continuous along the core sediments the distribution of realgar and orpiment appears to be uneven.

broadened peak at 2472 eV is assigned to the most reduced forms of S, native sulfur (S^0) and thiols; the second peak at 2481.2 eV is allocated to less reduced organic sulfur compounds, i.e. to sulfonates (S^{5+}); and the third peak is ascribed to the highly oxidized inorganic form of S, i.e. sulfate (S^{6+}) (Fig. 7). Furthermore, a shoulder also occurs at 2477.7–2478.5 eV in-between other absorption peaks, revealing the presence of sulfoxides (S^{+4}) (Fig. 7).

Overall, the S K-edge XANES spectra from MC04 and GC21 core samples display highly similar features, though with noticeable variations of the intensity absorption peaks of sulfates and sulfonates. Anyhow, the fitting results are unambiguous for sulfonates thanks to the clear separation in the absorption peaks between the S^{5+} oxidation state of sulfonates and the S^{6+} oxidation state of sulfate (Vairavamurthy et al., 1994; Xia et al., 1998). Moreover, the sulfate and sulfonates' compounds appear to be

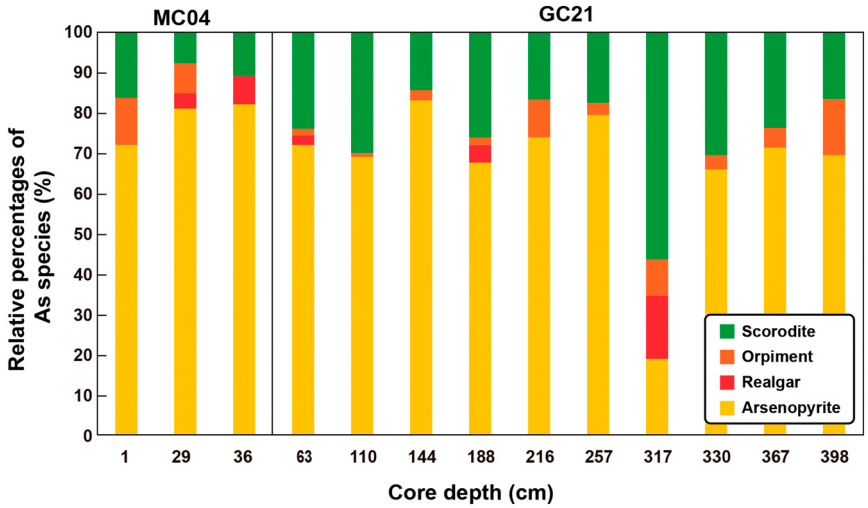

Fig. 6. Bar graphs showing relative percentages of the As species in the submarine mine tailings deposit obtained from LCF fittings. The relative percentage of As in arsenopyrite is maximum in sample MC04 36_37, corresponding to olive silts with 267–439 As ($mg{\cdot}kg^{-1}$). The relative percentage of As in scorodite and realgar peaks in sample GC21 317_318, corresponding to laminated orange to olive silts and black sandy silts with 184–366 As ($mg{\cdot}kg^{-1}$). In all samples, As can be found in orpiment with a maximum relative percentage in sample GC21 398_391, which corresponds to olive laminated silts with 515–751 As ($mg{\cdot}kg^{-1}$). The relative percentage of As in arsenopyrite and orpiment is higher in dark levels (i.e. olive silts, black sands and black sandy silts), whereas in scorodite and realgar the relative percentages of As are higher in orange levels (i.e. laminated orange silts).

anticorrelated in the submarine mine tailings. This is especially visible in the prominent sulfonate absorption band at 2473.4–2478.5 eV and the associated absence of the sulfate absorption band at 2483.12 eV in samples MC04 36_37, GC21_63_64 and GC21_398_399. What's more, the sulfonate distribution in the materials follows a non-systematic variation, which could be due, at least partly, to the turbulent nature of the anthropogenic dumping of the mine tailings and the associated trapping of organic debris in the deposits (Fig. 7) (Baza-Varas et al., 2022; Frigola et al., 2017).

5. Discussion

5.1. Arsenopyrite weathering

The open mining pits from Sierra Minera de Cartagena, with large volumes of exposed and oxidized sulfide ores, provide the right conditions for arsenopyrite oxidation (Dove and Rimstidt, 1985; Kerr et al., 2018; O'Day et al., 2004). It is well known that arsenopyrite oxidizes when

Table 1
Samples from Portman's Bay cores analyzed at ALBA synchrotron and fittings displaying the reference spectra from standard compounds and the amounts of the selected references that provide the best fit for each As—K XANES as a weighted sum (R-factor). Stratigraphic units are after Baza-Varas et al. (2022).

Core	Stratigraphic unit	Core depth (cm)	Unit description	Sample description	As ($mg{\cdot}kg^{-1}$)	Edge position (eV)	Arsenopyrite (%)	Realgar (%)	Orpiment (%)	Scorodite (%)
MC04	Unit 4	1–2	Massive dark grey to black sandy silts and fine sands with signs of bioturbation.	Grey sandy silts	266–438	11,866.8	71.6	–	11.6	15.7
	Unit 3	29–30	Massive olive, orange and greyish multicolored clays, silts and fine to medium sands with fining upwards sequences and other sedimentary structures. Includes black sands layers.	Olive silts	200–349	11,866.6	82.5	3.7	7.5	7.5
		36–37		Olive silts	267–439	11,866.6	84.1	7.2	–	10.4
GC21	Unit 3	63–64		Olive laminated silts	493–571	11,866.7	72.1	2.8	1.8	23.4
		110–111		Olive laminated silts	553–610	11,866.9	69.4	–	0.8	29.8
		144–145		Black laminated sandy silts	486–561	11,866.7	83.4	–	2.4	14.2
		188–189		Olive laminated silts	418–590	11,866.4	68.1	4.4	2	25.5
		216–217		Olive and orange laminated silts	441–665	11,866.7	74.2	–	9.6	16.3
		257–258		Black sands	212–271	11,866.5	79.7	–	2.9	17.3
		317–318		Laminated orange to olive silts and black sandy silts	184–366	11,866.8	19.1	16.2	8.9	55.7
		330–331		Laminated orange to olive silts and black sandy silts	270–318	11,866.7	66.2	–	2.8	31
		367–368		Olive laminated silts	588–967	11,866.7	71.8	–	4.7	23.5
		398–399		Olive laminated silts	515–751	11,866.4	69.9	–	13.7	16.4

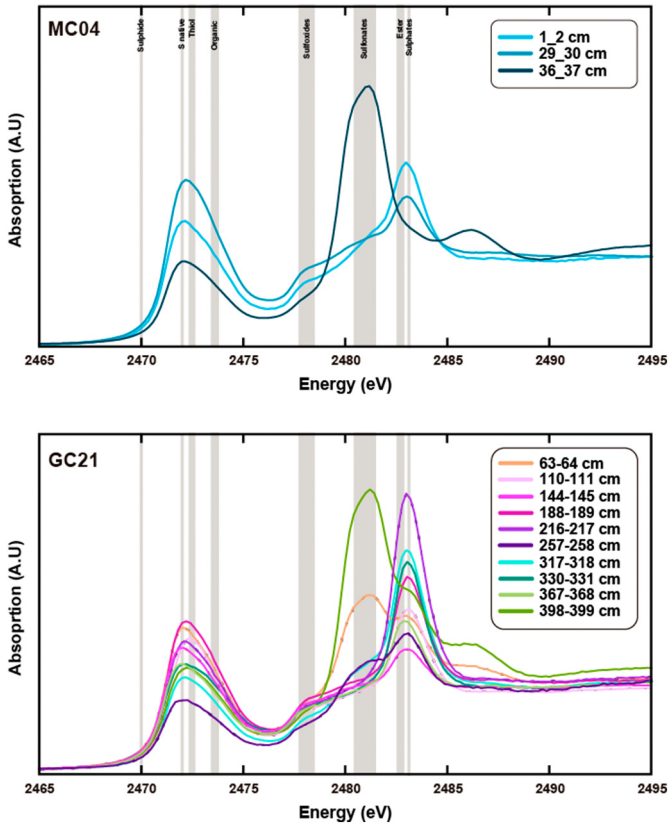

Fig. 7. The S K-edge XANES spectra with the highlighted maximum absorption peaks from the relative energy positions of representative soil sulfur compounds sulfide (S^{2-}) at 2470 eV, native sulfur (S^0) at 2472 eV, thiols at 2472.32–2472.65 eV, organic sulfides at 2473.4–2473.8 eV, sulfoxides (S^{4+}) at 2477.7–2478.5 eV, sulfonates (S^{5+}) at 2480.4–2481.5 eV, ester (S^{6+}) at 2482.5–2482.9 eV after (Solomon et al., 2011) and gypsum (S^{6+}) at 2483.12 eV. On MC04 sediment core subsamples from both units 3 and 4 the first absorption intensity peak at low energies is just above native sulfur and shifted towards thiols with a visible broadening associated to sulfoxides; the second absorption intensity peak at higher energies corresponds to sulfate but on Unit 3 samples it appears at lower energies and corresponds to sulfonate. On GC21 sediment core subsamples the first absorption intensity peak at low energies is also just above native sulfur and shifted towards thiols with a visible broadening associated to sulfoxides; the second absorption intensity peak at higher energies corresponds to sulfate though in some samples at lower energies and corresponds to sulfonate.

exposed to air, forming a submicron overlayer, known as “tarnish”, made of Fe and As oxides (Corkhill and Vaughan, 2009; Diacomanolis et al., 2016; Nesbitt et al., 1995). When exposed to water, the oxidation process of arsenopyrite accelerates, leading to the development of an oxidized overlayer constituted mostly by As oxides and sulfate (Corkhill and Vaughan, 2009). Under more acidic conditions, such an oxidized overlayer consists of scorodite and minor amounts of elemental S (Corkhill and Vaughan, 2009; Costa et al., 2002; Mikhlin and Tomashevich, 2005). The development of this oxidized overlayer would protect arsenopyrite grains from dissolution during ore treatment and accumulation on Portmán's Bay seabed where the submarine mine tailings deposit was developing (Corkhill and Vaughan, 2009; Craw et al., 2003). In effect, the arsenopyrite grains in the investigated core samples show sharp edges and flat crystal faces with no evidence of chemical corrosion, despite of having been underwater for >30 years (Fig. 3). Consequently, the arsenopyrite is expected to endure with negligible decomposition within the submarine mine tailings. This is in agreement with the abundant presence of arsenopyrite and lesser amounts of scorodite in the core samples, as determined from the speciation of As (Fig. 6 and Table 1).

Besides, in the presence of acid rock drainage in the open mine pits, realgar and orpiment could already occur in Sierra Minera de Cartagena ores (Kerr et al., 2018; O'Day et al., 2004). Under these conditions thermodynamic data predicts for realgar and orpiment to develop and replace arsenopyrite (Corkhill and Vaughan, 2009; Craw et al., 2003). However, the available evidence suggests that this is unlikely, with realgar and orpiment forming as micron sized precipitates instead (Corkhill and Vaughan, 2009; Craw et al., 2003; Kerr et al., 2018). Nevertheless, would they be already present, neither realgar nor orpiment would have survived the oxidizing and alkaline conditions during their transport and deposition on Portman's Bay seabed (Craw et al., 2003; Kerr et al., 2018; O'Day et al., 2004). Hence, our hypothesis to explain the presence of realgar and orpiment in the submarine mine tailings is that they are authigenic. The presence of scorodite and its decomposition in a reducing environment would provide the suitable As-rich medium for realgar and orpiment to precipitate (Álvarez-Ayuso, 2021; Dove and Rimstidt, 1985; Kerr et al., 2018; Nesbitt et al., 1995). This view is supported by the simultaneous presence of arsenopyrite, scorodite, realgar and orpiment in the core samples as determined, again, from the results of As speciation analyses (Figs. 5, 6 and Table 1).

5.2. As and S biogeochemistry

The impact of SRB activity in the submarine mine waste deposit deserves special attention, since SRB are often involved in the formation of realgar and orpiment in As-rich mine tailings (Kerr et al., 2018; Le Pape et al., 2017; Miot et al., 2009; Newman et al., 1997; O'Day et al., 2004; Sun et al., 2019). The speciation of S in our core samples confirms the simultaneous presence of a range of inorganic and organic sulfur compounds, such as elemental sulfur, thiols, sulfoxides and sulfonates, which are commonly related to the activity of SRB (Jørgensen et al., 2019; Lie et al., 1996; Vairavamurthy et al., 1994) (Fig. 7). Elemental sulfur can result from sulfide oxidation by SRB for energy storage purposes (Jørgensen, 2021; Jørgensen et al., 2019; Vairavamurthy et al., 1994). Reduced organic sulfur compounds, such as thiols, commonly result from a sulfate reductive assimilation process by SRB. These compounds are of special relevance since they have a high affinity with As and are thought to be involved in As reduction (Le Pape et al., 2017; Miot et al., 2009; Newman et al., 1997). The presence of more oxidized organic sulfur compounds, such as sulfonates and sulfoxides, would result from the entrapment of vegetal fibers and other organic debris from the lush seagrass meadows that once covered the seafloor of the study area (Baza-Varas et al., 2022; Jørgensen et al., 2019; Kertesz, 2000; Manteca et al., 2014; Oyarzun et al., 2013; Peřestá et al., 2022; Vairavamurthy et al., 1994). The presence of sulfonates is particularly appealing as they represent sulfur, carbon and energy sources needed for the SRB metabolism (Jørgensen, 2021; Lie et al., 1996; Peřestá et al., 2022; Ruiz et al., 2015b; Vairavamurthy et al., 1994).

Hence, the simultaneous occurrence of organic sulfur compounds and As-sulfides supports the development of authigenic realgar and orpiment associated to SRB activity in Portman's Bay submarine mine tailings (Kertesz, 2000; Lie et al., 1996; Vairavamurthy et al., 1994). This is in agreement with the obvious (and measured) presence of organic matter in the investigated cores, including large-sized vegetal remnants and dark colors typical of organic matter loaded deposits, therefore defining a favourable environment for SRB to thrive (Figs. 1 and 7) (Alam and McPhedran, 2019; Baza-Varas et al., 2022; Drahota et al., 2017; Kerr et al., 2018; Rodriguez-Freire et al., 2016). Realgar and orpiment would consist of tiny and disseminated particles, stable under the reducing conditions —with a measured interstitial water pH of 6— of the submarine mine tailings deposit (Alam and McPhedran, 2019; Kerr et al., 2018; Le Pape et al., 2017; Newman et al., 1997). The precipitation of tiny (submicron) realgar and orpiment particles by SRB has been proposed as an effective removal mechanism of As in heavily contaminated waters and mine tailings (Briones-Gallardo et al., 2017; Drahota et al., 2017; Gadd, 2010; Kerr et al., 2018; Le Pape et al., 2017). The submicron size of realgar and orpiment particles would explain the non-observation of realgar and orpiment grains of convenient size in the examined samples.

5.3. As ecotoxicology and bioavailability

Whereas As concentrations in uncontaminated soils typically range from 1 to 40 mg kg^{-1} (Álvarez-Ayuso, 2021; Neff, 1997), in Portmán's Bay submarine mine tailings they are as high as 2775 mg kg^{-1} (Baza-Varas et al., 2022), which should raise concern since As is a serious toxicant (Alam and McPhedran, 2019). Understanding the As bioavailability in Portmán's Bay submarine mine tailings deposit —and in similar deposits worldwide— is, therefore, of the utmost importance (García-lorenzo et al., 2014; Martínez-Gómez et al., 2012; Mestre et al., 2017). As^{5+} and As^{3+} are the dominant forms of inorganic As, with As^{3+} presenting a higher mobility and toxicity than As^{5+} in marine ecosystems (Gbaruko et al., 2008). As remediation technologies generally rely on either changing its oxidation state from one form to another, or on converting it into insoluble compounds that precipitate out from water (Alam and McPhedran, 2019; Le Pape et al., 2017). Besides, the most novel As remediation techniques and proposals preferentially address the most unstable As-bearing mineral phases, such as amorphous ferric arsenates, and their weathering (Álvarez-Ayuso, 2021; Paktunc and Bruggeman, 2010; Wang et al., 2019). However, no technique for As removal or chemical stabilization was ever employed in Portman's Bay floatation plant, which further stresses the relevance of properly characterizing the submarine mine tailings and emphasizes the interest of understanding the environmental fate of As in such a submarine setting.

Our data indicates that the arsenopyrite in Portmán's submarine mine tailings is partially oxidized (Craw et al., 2003; Manteca et al., 2014; Oyarzun et al., 2013), which implies the development of a protective oxidized overlayer precluding arsenopyrite from dissolution (Craw et al., 2003; O'Day et al., 2004). However, the arsenopyrite's oxidized overlayer may dissolve under the more reducing conditions within the submarine mine tailings, releasing As^{+5} that subsequently, in presence of organic matter, would reduce to As^{2+} and As^{3+} and react with sulfide through the mediation of SRB. The immobilization of As in the form of authigenic realgar and orpiment would lead to a massive As removal in response to the immobilization of highly toxic As^{3+} by the activity of SRB (Drahota et al., 2017; Eberle et al., 2020; Falteisek et al., 2020; Jørgensen et al., 2019; Knappová et al., 2019; Le Pape et al., 2017; Peřestá et al., 2022). Nevertheless, the precipitation, stability and sorption of authigenic realgar and orpiment should be further inspected to better assess and predict the As precipitation rates and mobility in Portmán's Bay submarine mine tailings and beyond. Besides, it should be highlighted that this is this first time that sulfonates are found in submarine mine tailings, hence opening new perspectives on the sulfur biogeochemical cycle in heavy metal and metalloid polluted marine environments (Vairavamurthy et al., 1994).

The present study provides valuable insight about As and S biogeochemistry in submarine mine tailings deposits (Kertesz, 2000; Lie et al., 1996; Martínez-Gómez et al., 2012; Neff, 1997; Vairavamurthy et al., 1994). It should be taken into account that while the near-shore part of Portmán's Bay mine tailings deposit clearly is an environmental disaster, under the current conditions its offshore extension can be viewed as less of an issue and may be best left alone. What is more, the offshore part of the tailings, may provide useful lessons for other marine disposal systems that involve high contents of As, such as weighting the convenience of pumping the tailings farther and deeper so that burial of near-shore habitats —as in Portmán's case— is prevented. However, this view must not be taken as an advocacy for dumping mine tailings into the sea, but as a matter of fact that should be assessed, amongst other options, by appropriate environmental impact assessments on a case-by-case basis prior to any dumping. The Portmán's Bay submarine mine tailings deposit still offers plenty of opportunities beyond the present work to improve current knowledge on underwater As-bearing waste piles. These could include, for instance, a comparison between onshore tailings accumulations and their potential environmental effects (e.g., acid rock drainage) versus offshore deposition that soaks the tailings in marine waters. Further XAS experiments and the detailed study of the interstitial waters within the submarine mine tailings would be critical to further research.

6. Conclusions

Portman's submarine mine tailings contain significant amounts of As, amongst other toxic elements, which has important environmental implications (Cerdà-Domènech et al., 2018; Mestre et al., 2017; Neff, 1997). Our results suggest that As in the submarine mine tailings is affected by a combination of inorganic and organic geochemical processes. As speciation analyses allowed identifying the presence and distribution of arsenopyrite, scorodite, realgar and orpiment, while S speciation analyses allowed determining the presence and distribution of inorganic and organic sulfur compounds associated to the activity of SRB. Hence, for the first-time valuable hints on the formation of authigenic realgar and orpiment in submarine sulfide mine tailings is provided.

The collected evidence indicates that, due to oxidation, arsenopyrite grains developed an oxidized overlayer or “tarnish” protecting them from dissolution during ore treatment, transport to the discharge point and accumulation onto the seafloor. The arsenopyrite's oxidized overlayer results in the oxidation of As^{-1} and the production of As^{+5} in scorodite following Eq. (1).

$$FeAsS + 14Fe^{+5} + 10H_2O -> 14Fe^{+2} + SO_4{}^{-2} + FeAsO_4 \cdot 2H_2O \quad (1)$$

The resulting scorodite can then dissolve under the more reducing conditions within the submarine mine tailings, which may lead to the release of As^{+5} as shown in Eq. (2).

$$FeAsO_4 \cdot 2H_2O -> FeOOH + H_2AsO_4{}^{-} + H^{+} \quad (2)$$

Subsequently, the As^{+5} can reduce to As^{+3} using electron donors from the organic matter in the deposit, subsequently resulting in the precipitation of orpiment eased by SRB activity (Briones-Gallardo et al., 2017; Kirk et al., 2010; Le Pape et al., 2017). Furthermore, the observed reduction to As^{+2} and the precipitation of realgar would be also driven by the presence of biogenic H_2S as shown in Eqs. (3) and (4).

$$2H_3AsO_3 + 3H_2S -> As_2S_3 + 6H_2O \quad (3)$$

$$As_2S_3 + H_2S -> 2AsS + H_2S_2 \quad (4)$$

The presence of elemental sulfur, thiols, sulfonates and sulfate across the studied samples evidences the activity of SRB in the submarine mine tailings, and thus offers a trustworthy explanation to the reactions leading to the formation of authigenic realgar and orpiment. It is to be noticed that the results and interpretations here presented go beyond previous assumptions about the mineralogy and geochemistry od submarine sulfide mine tailings, which hindered the complexity of the As biogeochemistry in polluted marine environments (Alorda-Kleinglass et al., 2019; Baza-Varas et al., 2022; Cerdà-Domènech et al., 2019; Frigola et al., 2017; Herath et al., 2016; Palau et al., 2021).

Our findings are of high relevance for the Portmán case and beyond. Partial removal of inshore mine tailings in Portmán Bay has been carried out in the frame of remediation works. The eventual expansion of removal operations to the offshore extension of the mine tailings deposit, where most of its volume is, would resuspend huge amounts of particles, with the risk of releasing currently immobilized As to the marine environment, thus largely enhancing their bioavailability and ensuing ecotoxicological impacts, at least temporarily. The spreading of suspensates far beyond the dumping site can further expand the impact of such activities to more distant areas. The present study also provides fundamental insight would removal techniques such as dredging, suction or other mechanical methods be envisaged for similar settings all over the world for remediation purposes and points to the need of weighing the widest possible span of options, including sealing of the mine tailings deposits and no action, on a case by case basis.

Supplementary data to this article can be found online at https://doi.org/10.1016/j.scitotenv.2023.163649.

CRediT authorship contribution statement

Josep Roqué-Rosell: Conceptualization, Methodology, Formal analysis, Investigation, Data curation, Visualization, Writing – original draft. Andrea Baza-Varas: Conceptualization, Methodology, Formal analysis, Investigation, Data curation, Visualization, Writing – original draft. Miquel Canals: Conceptualization, Funding acquisition, Project administration, Supervision, Writing – review and editing. Jaime Frigola: Data Curation, Supervision, Writing – review and editing. Marc Cerda-Domènech: Methodology, Data Curation. Anna Sanchez-Vidal: Conceptualization, Project administration, Methodology, Supervision. David Amblàs: Methodology, Data Curation. M. Campeny: Providing mineral standards. C. Marini: Methodology, Data Curation.

Data availability

Data will be made available on request.

Declaration of competing interest

This manuscript has not been published and is not under consideration for publication elsewhere. We have no conflicts of interest to disclose.

Acknowledgements

This research has been carried out as part of the NUREIEVA research project (ref. CTM2016-75953-C2-1-R) funded by the Spanish Government, and a Catalan Government *Grups de Recerca Consolidats* (excellence research groups) grant to GRC *Geociències Marines* (ref. 2017 SGR 315). It is also a contribution of the Sustainable Blue Economy Chair of the University of Barcelona. A.B.V. got financial support from an APIF PhD fellowship from the University of Barcelona. J.F. acknowledges the Serra Húnter Programme of Generalitat de Catalunya for funding him a tenure-eligible lecturer contract. We would like to thank the crew of R/V Ángeles Alvariño and all scientific and technical staff involved in the NUREIEV-3 and NUREIEVA-MAR1 research cruises. We also thank the ALBA synchrotron facility for providing CLAESS beamtime for XAS. Finally, we would also like to thank Carlos Pedrós-Alió from the *Centro Nacional de Biotecnología*, CSIC, in Madrid, and Prof. Anicet Ramon Blanch from the *Departament de Genètica, Microbiologia i Estadística* of University of Barcelona for their valuable comments and observations. We sincerely appreciate the comments and criticisms made to earlier versions of the paper by four reviewers, which greatly helped to improve it. Special thanks go to Prof. Dave Craw from the University of Otago, New Zealand, whose persistent and to the point comments pushed us to better substantiate the most debated aspects in the paper.

References

Acosta, J., Fontán, A., Muñoz, A., Muñoz-Martín, A., Rivera, J., Uchupi, E., 2013. The morphotectonic setting of the Southeast margin of Iberia and the adjacent oceanic Algero-Balearic Basin. Mar. Pet. Geol. 45, 17–41. https://doi.org/10.1016/j.marpetgeo.2013.04.005.

Alam, R., McPhedran, K., 2019. Applications of biological sulfate reduction for remediation of arsenic – a review. Chemosphere 222, 932–944. https://doi.org/10.1016/j.chemosphere.2019.01.194.

Alorda-Kleinglass, A., Garcia-Orellana, J., Rodellas, V., Cerdà-Domènech, M., Tovar-Sánchez, A., Diego-Feliu, M., Trezzi, G., Sánchez-Quilez, D., Sanchez-Vidal, A., Canals, M., 2019. Remobilization of dissolved metals from a coastal mine tailing deposit driven by groundwater discharge and porewater exchange. Sci. Total Environ. 688, 1359–1372. https://doi.org/10.1016/j.scitotenv.2019.06.224.

Álvarez-Ayuso, E., 2021. Stabilization and encapsulation of arsenic-/antimony-bearing mine waste: overview and outlook of existing techniques. Crit. Rev. Environ. Sci. Technol., 1–33 https://doi.org/10.1080/10643389.2021.1944588.

Auernheimer, C., Chinchon, S., 1997. Calcareous skeletons of sea urchins as indicators of heavy metals pollution. Portman Bay, Spain. Environ. Geol. https://doi.org/10.1007/s002540050106.

Baza-Varas, A., Canals, M., Frigola, J., Cerdà-Domènech, M., Rodés, N., Tarrés, M., Sanchez-Vidal, A., 2022. Multiproxy characterization of sedimentary facies in a submarine sulphide mine tailings dumping site and their environmental significance: the study case of Portmán Bay (SE Spain). Sci. Total Environ. 810, 151183. https://doi.org/10.1016/j.scitotenv.2021.151183.

Benedicto, J., Andral, B., Martínez-Gómez, C., Guitart, C., Deudero, S., Cento, A., Scarpato, A., Caixach, J., Benbrahim, S., Chouba, L., Boulahdid, M., Galgani, F., 2011. A large scale survey of trace metal levels in coastal waters of the Western Mediterranean basin using caged mussels (Mytilus galloprovincialis). J. Environ. Monit. https://doi.org/10.1039/c0em00725k.

Briones-Gallardo, R., Escot-Espinoza, V.M., Cervantes-González, E., 2017. Removing arsenic and hydrogen sulfide production using arsenic-tolerant sulfate-reducing bacteria. Int. J. Environ. Sci. Technol. 14, 609–622. https://doi.org/10.1007/s13762-016-1174-1.

Cerdà-Domènech, M., Frigola, J., Sanchez-Vidal, Amblas, D., Canals, M., Rodes, N., Amate, R., 2018. Multi-proxy characterization of the coastal mine tailings of Portmán Bay, SE Spain. VI International Symposium on Marine Sciences Vigo (Spain), p. 437.

Cerdà-Domènech, M., Frigola, J., Sanchez-Vidal, A., Canals, M., 2019. Calibrating high resolution XRF core scanner data to obtain absolute metal concentrations in highly polluted marine deposits after two case studies off Portmán Bay and Barcelona,Spain. Sci. Total Environ. 134778. https://doi.org/10.1016/j.scitotenv.2019.134778.

Collins, P.C., Croot, P., Carlsson, J., Colaço, A., Grehan, A., Hyeong, K., Kennedy, R., Mohn, C., Smith, S., Yamamoto, H., Rowden, A., 2013. A primer for the environmental impact assessment of mining at seafloor massive sulfide deposits. Mar. Policy 42, 198–209. https://doi.org/10.1016/j.marpol.2013.01.020.

Corkhill, C.L., Vaughan, D.J., 2009. Arsenopyrite oxidation – a review. Appl. Geochem. 24, 2342–2361. https://doi.org/10.1016/j.apgeochem.2009.09.008.

Costa, M., Botelho do Rego, A., Abrantes, L., 2002. Characterization of a natural and an electro-oxidized arsenopyrite: a study on electrochemical and X-ray photoelectron spectroscopy. Int. J. Miner. Process. 65, 83–108. https://doi.org/10.1016/S0301-7516(01)00059-X.

Craw, D., Falconer, D., Youngson, J.H., 2003. Environmental arsenopyrite stability and dissolution: theory, experiment, and field observations. Chem. Geol. 199, 71–82. https://doi.org/10.1016/S0009-2541(03)00117-7.

Cullen, W.R., Reimer, K.J., 1989. Arsenic speciation in the environment. Chem. Rev. 89, 713–764. https://doi.org/10.1021/cr00094a002.

Diacomanolis, V., Noller, B.N., Taga, R., Harris, H.H., Aitken, J.B., Ng, J.C., 2016. Relationship of arsenic speciation and bioavailability in mine wastes for human health risk assessment. Environ. Chem. 13, 641–655. https://doi.org/10.1071/EN14152.

Domènech, C., De Pablo, J., Ayora, C., 2002. Oxidative dissolution of pyritic sludge from the Aznalcóllar mine (SW Spain). Chem. Geol. 190, 339–353. https://doi.org/10.1016/S0009-2541(02)00124-9.

Dove, P.M.M., Rimstidt, J.D., 1985. The solubility and stability of scorodite, FeAsO4.2H2O. Am. Mineral. 70, 838–844.

Drahota, P., Mikutta, C., Falteisek, L., Duchoslav, V., Klementová, M., 2017. Biologically induced formation of realgar deposits in soil. Geochim. Cosmochim. Acta 218, 237–256. https://doi.org/10.1016/j.gca.2017.09.023.

Eberle, A., Besold, J., Kerl, C.F., Lezama-Pacheco, J.S., Fendorf, S., Planer-Friedrich, B., 2020. Arsenic fate in peat controlled by the pH-dependent role of reduced sulfur. Environ. Sci. Technol. 54, 6682–6692. https://doi.org/10.1021/acs.est.0c00457.

Embile, R.F., Walder, I.F., Schuh, C., Donatelli, J.L., 2018. Cu, Pb and Fe release from sulfide-containing tailings in seawater: results from laboratory simulation of submarine tailings disposal. Mar. Pollut. Bull. 137, 582–592. https://doi.org/10.1016/j.marpolbul.2018.11.012.

Falteisek, L., Drahota, P., Culka, A., Laufek, F., Trubač, J., 2020. Bioprecipitation of As4S4 polymorphs in an abandoned mine adit. Appl. Geochem. 113. https://doi.org/10.1016/j.apgeochem.2019.104511.

Farquhar, M.L., Charnock, J.M., Livens, F.R., Vaughan, D.J., 2002. Mechanisms of arsenic uptake from aqueous solution by interaction with goethite, lepidocrocite, mackinawite, and pyrite: an X-ray absorption spectroscopy study. Environ. Sci. Technol. 36, 1757–1762. https://doi.org/10.1021/es010216g.

Foster, A.L., Brown, G.E., Tingle, T.N., Parks, G.A., 1998. Quantitative arsenic speciation in mine tailings using X-ray absorption spectroscopy. Am. Mineral. 83, 553–568. https://doi.org/10.2138/am-1998-5-616.

Frigola, J., Cerdà-domènech, M., Barriuso, E., Sanchez-vidal, A., Amblas, D., Canals, M., 2017. Micro CT characterization of a coastal mine tailings deposit. Portmán 19, 18096.

Gadd, G.M., 2010. Metals, minerals and microbes: geomicrobiology and bioremediation. Microbiology 156, 609–643. https://doi.org/10.1099/mic.0.037143-0.

García-lorenzo, M.L., Pérez-sirvent, C., Molina-ruiz, J., Martínez-sánchez, M.J., 2014. Mobility indices for the assessment of metal contamination in soils affected by old mining activities. J. Geochem. Explor. 147, 117–129. https://doi.org/10.1016/j.gexplo.2014.06.012.

Gbaruko, B.C., Ana, G.R.E.E., Nwachukwu, J.K., 2008. Ecotoxicology of arsenic in the hydrosphere: implications for public health. Afr. J. Biotechnol. 7, 4737–4742.

Herath, I., Vithanage, M., Bundschuh, J., Maity, J.P., Bhattacharya, P., 2016. Natural arsenic in global groundwaters: distribution and geochemical triggers for mobilization. Curr. Pollut. Rep. 2, 68–89. https://doi.org/10.1007/s40726-016-0028-2.

Hopp, L., Nico, P.S., Marcus, M.A., Peiffer, S., 2008. Arsenic and chromium partitioning in a podzolic soil contaminated by chromated copper arsenate. Environ. Sci. Technol. 42, 6481–6486. https://doi.org/10.1021/es800615f.

Hudson-Edwards, K., 2016. Tackling mine wastes. Science 352, 288–290. https://doi.org/10.1126/science.aaf3354.

Huerta-Diaz, M.A., Morse, J.W., 1992. Pyritization of trace metals in anoxic marine sediments: RN - Geochim. Cosmochim. Acta, v. 56, p. 2681–2702. Geochim. Cosmochim. Acta 56, 2681–2702.

Hughes, D.J., Shimmield, T.M., Black, K.D., Howe, J.A., 2015. Ecological impacts of large-scale disposal of mining waste in the deep sea. Sci. Rep. 5, 9985. https://doi.org/10.1038/srep09985.

Hunter, J.D., 2007. Matplotlib: a 2D graphics environment. Comput. Sci. Eng. 9, 90–95. https://doi.org/10.1109/MCSE.2007.55.

Jørgensen, B.B., 2021. Sulfur biogeochemical cycle of marine sediments. Geochem. Perspect. 10, 145–307. https://doi.org/10.7185/geochempersp.10.2.
Jørgensen, B.B., Findlay, A.J., Pellerin, A., 2019. The biogeochemical sulfur cycle of marine sediments. Front. Microbiol. 10, 1–27. https://doi.org/10.3389/fmicb.2019.00849.
Kalia, K., Khambholja, D.B., 2015. Arsenic contents and its biotransformation in the marine environment. In: Flora, S.J.S.B.T.-H. of A.T. (Ed.), Handbook of Arsenic Toxicology. Elsevier, Oxford, pp. 675–700 https://doi.org/10.1016/B978-0-12-418688-0.00028-9.
Kerr, G., Craw, D., Trumm, D., Pope, J., 2018. Authigenic realgar and gold in dynamic redox gradients developed on historic mine wastes,New Zealand. Appl. Geochem. 97, 123–133. https://doi.org/10.1016/j.apgeochem.2018.08.009.
Kertesz, M.A., 2000. Riding the sulfur cycle - metabolism of sulfonates and sulfate esters in Gram-negative bacteria. FEMS Microbiol. Rev. 24, 135–175. https://doi.org/10.1016/S0168-6445(99)00033-9.
Kirk, M.F., Roden, E.E., Crossey, L.J., Brealey, A.J., Spilde, M.N., 2010. Experimental analysis of arsenic precipitation during microbial sulfate and iron reduction in model aquifer sediment reactors. Geochim. Cosmochim. Acta 74, 2538–2555. https://doi.org/10.1016/j.gca.2010.02.002.
Knappová, M., Drahota, P., Falteisek, L., Culka, A., Penížek, V., Trubač, J., Mihaljevič, M., Matoušek, T., 2019. Microbial sulfidogenesis of arsenic in naturally contaminated wetland soil. Geochim. Cosmochim. Acta 267, 33–50. https://doi.org/10.1016/j.gca.2019.09.021.
Koski, R., 2012. Metal dispersion resulting from mining activities in coastal environments: a pathways approach. Oceanography 25, 170–183. https://doi.org/10.5670/oceanog.2012.53.
Last, W.M., Smol, J.P., 2002. In: Last, W.M., Smol, J.P. (Eds.), Tracking Environmental Change Using Lake Sediments. Developments in Paleoenvironmental Research1. Springer, Dordrecht. https://doi.org/10.1007/0-306-47669-X_1.
Le Pape, P., Battaglia-Brunet, F., Parmentier, M., Joulian, C., Gassaud, C., Fernandez-Rojo, L., Guigner, J.M., Ikogou, M., Stetten, L., Olivi, L., Casiot, C., Morin, G., 2017. Complete removal of arsenic and zinc from a heavily contaminated acid mine drainage via an indigenous SRB consortium. J. Hazard. Mater. 321, 764–772. https://doi.org/10.1016/j.jhazmat.2016.09.060.
Lie, T.J., Pitta, T., Leadbetter, E.R., Godchaux III, W., Leadbetter, J.R., 1996. Sulfonates: novel electron acceptors in anaerobic respiration. Arch. Microbiol. 166, 204–210. https://doi.org/10.1007/s002030050376.
Manceau, A., Lanson, M., Geoffroy, N., 2007. Natural speciation of Ni, Zn, Ba, and As in ferromanganese coatings on quartz using X-ray fluorescence, absorption, and diffraction. Geochim. Cosmochim. Acta 71, 95–128. https://doi.org/10.1016/j.gca.2006.08.036.
Manteca, J.I., García, J.Á.L., Oyarzun, R., Carmona, C., 2014. The beach placer iron deposit of Portman Bay, Murcia, SE Spain: the result of 33 years of tailings disposal (1957–1990) to the Mediterranean seaside. Miner. Depos. 49, 777–783. https://doi.org/10.1007/s00126-014-0511-x.
Marcus, M.A., Manceau, A., Kersten, M., 2004. Mn, Fe, Zn and As speciation in a fast-growing ferromanganese marine nodule. Geochim. Cosmochim. Acta 68, 3125–3136. https://doi.org/10.1016/j.gca.2004.01.015.
Martínez-Gómez, C., Fernández, B., Benedicto, J., Valdés, J., Campillo, J.A., León, V.M., Vethaak, A.D., 2012. Health status of red mullets from polluted areas of the Spanish Mediterranean coast, with special reference to Portmán (SE Spain). Mar. Environ. Res. 77, 50–59. https://doi.org/10.1016/j.marenvres.2012.02.002.
McKinney, W., 2010. Data Structures for Statistical Computing in Python. Proc. 9th Python Sci. Conf.
Mestre, N.C., Rocha, T.L., Canals, M., Cardoso, C., Danovaro, R., Dell'Anno, A., Gambi, C., Regoli, F., Sanchez-Vidal, A., Bebianno, M.J., 2017. Environmental hazard assessment of a marine mine tailings deposit site and potential implications for deep-sea mining. Environ. Pollut. 228, 169–178. https://doi.org/10.1016/j.envpol.2017.05.027.
Mikhlin, Y., Tomashevich, Y., 2005. Pristine and reacted surfaces of pyrrhotite and arsenopyrite as studied by X-ray absorption near-edge structure spectroscopy. Phys. Chem. Miner. 32, 19–27. https://doi.org/10.1007/s00269-004-0436-5.
Miot, J., Morin, G., Skouri-Panet, F., Férard, C., Poitevin, A., Aubry, E., Ona-Nguema, G., Juillot, F., Guyot, F., Brown, G.E., 2009. Speciation of arsenic in Euglena gracilis cells exposed to As(V). Environ. Sci. Technol. 43, 3315–3321. https://doi.org/10.1021/es802833s.
Moore, J.N., Ficklin, W.H., Johns, C., 1988. Partitioning of arsenic and metals in reducing sulfidic sediments. Environ. Sci. Technol. 22, 432–437. https://doi.org/10.1021/es00169a011.
Mosselmans, J.F.W., Quinn, P.D., Roque Rosell, J., Atkinson, K.D., Dent, A.J., Cavill, S.I., Hodson, M.E., Kirk, C.A., Schofield, P.F., 2008. The first environmental science experiments on the new microfocus spectroscopy beamline at diamond. Mineral. Mag. 72, 197–200. https://doi.org/10.1180/minmag.2008.072.1.197.
Mosselmans, J.F.W.F.W., Quinn, P.D., Dent, A.J., Cavill, S.A., Moreno, S.D., Peach, A., Leicester, P.J., Keylock, S.J., Gregory, S.R., Atkinson, K.D., Rosell, J.R., 2009. I18 – the microfocus spectroscopy beamline at the Diamond Light Source. J. Synchrotron Radiat. 16, 818–824. https://doi.org/10.1107/S0909049509032282.
Neff, J.M., 1997. Ecotoxicology of arsenic in the marine environment. Environ. Toxicol. Chem. 16, 917–927. https://doi.org/10.1002/etc.5620160511.
Nesbitt, H.W., Muir, I.J., Prarr, A.R., 1995. Oxidation of arsenopyrite by air and air-saturated, distilled water, and implications for mechanism of oxidation. Geochim. Cosmochim. Acta 59, 1773–1786. https://doi.org/10.1016/0016-7037(95)00081-A.
Newman, D.K., Beveridge, T.J., Morel, F., 1997. Precipitation of arsenic trisulfide by Desulfotomaculum auripigmentum. Appl. Environ. Microbiol. 63, 2022–2028. https://doi.org/10.1128/aem.63.5.2022-2028.1997.
Nicholas, S.L., Erickson, M.L., Woodruff, L.G., Knaeble, A.R., Marcus, M.A., Lynch, J.K., Toner, B.M., 2017. Solid-phase arsenic speciation in aquifer sediments: a micro-X-ray absorption spectroscopy approach for quantifying trace-level speciation. Geochim. Cosmochim. Acta 211, 228–255. https://doi.org/10.1016/j.gca.2017.05.018.
O'Day, P.A., Vlassopoulos, D., Root, R., Rivera, N., 2004. The influence of sulfur and iron on dissolved arsenic concentrations in the shallow subsurface under changing redox conditions. Proc. Natl. Acad. Sci. 101, 13703–13708. https://doi.org/10.1073/pnas.0402775101.
Oremland, R.S., Stolz, J.F., 2003. The ecology of arsenic. Science 300, 939–944. https://doi.org/10.1126/science.1081903.
Oyarzun, R., Manteca Martínez, J.I., López García, J.A., Carmona, C., 2013. An account of the events that led to full bay infilling with sulfide tailings at Portman (Spain), and the search for "black swans" in a potential land reclamation scenario. Sci. Total Environ. 454–455, 245–249. https://doi.org/10.1016/j.scitotenv.2013.03.030.
Paktunc, D., 2013. Mobilization of arsenic from mine tailings through reductive dissolution of goethite influenced by organic cover. Appl. Geochem. 36, 49–56. https://doi.org/10.1016/j.apgeochem.2013.05.012.
Paktunc, D., Bruggeman, K., 2010. Solubility of nanocrystalline scorodite and amorphous ferric arsenate: implications for stabilization of arsenic in mine wastes. Appl. Geochem. 25, 674–683. https://doi.org/10.1016/j.apgeochem.2010.01.021.
Palau, J., Benaiges-Fernandez, R., Offeddu, F., Urmeneta, J., Soler, J.M., Cama, J., Dold, B., 2021. Release of trace elements during bioreductive dissolution of magnetite from metal mine tailings: potential impact on marine environments. Sci. Total Environ. 788, 147579. https://doi.org/10.1016/j.scitotenv.2021.147579.
Peřestá, M., Drahota, P., Culka, A., Matoušek, T., Mihaljevič, M., 2022. Impact of organic matter on as sulfidation in wetlands: an in situ experiment. Sci. Total Environ. 819. https://doi.org/10.1016/j.scitotenv.2021.152008.
Pfeifer, H.R., Gueye-Girardet, A., Reymond, D., Schlegel, C., Temgoua, E., Hesterberg, D.L., Chou, J.W., 2004. Dispersion of natural arsenic in the Malcantone watershed, Southern Switzerland: field evidence for repeated sorption-desorption and oxidation-reduction processes. Geoderma 122, 205–234. https://doi.org/10.1016/j.geoderma.2004.01.009.
Ramirez-llodra, E., Cecilie, H., Andersen, G.S., Baeten, N.J., Gundersen, H., Arne, R., Brooks, S.J., Escudero-o, C., Ibragimova, O., Lepland, A., Nepstad, R., Sand, R., Thorne, M., Shimmield, T., Yakushev, E., Ferrando-climent, L., Helge, P., 2022. New Insights Into Submarine Tailing Disposal for a Reduced Environmental Footprint: Lessons Learnt From Norwegian Fjords, p. 174 https://doi.org/10.1016/j.marpolbul.2021.113150.
Ravel, B., Newville, M., 2005. ATHENA and ARTEMIS interactive graphical data analysisusing IFEFFIT. Phys. Scr. 1007. https://doi.org/10.1238/Physica.Topical.115a01007.
Rodriguez-Freire, L., Moore, S.E., Sierra-Alvarez, R., Root, R.A., Chorover, J., Field, J.A., 2016. Arsenic remediation by formation of arsenic sulfide minerals in a continuous anaerobic bioreactor. Biotechnol. Bioeng. 113, 522–530. https://doi.org/10.1002/bit.25825.
Roqué-Rosell, J., Villanova-de-Benavent, C., Proenza, J.A., 2017. The accumulation of Ni in serpentines and garnierites from the Falcondo Ni-laterite deposit (Dominican Republic) elucidated by means of μXAS. Geochim. Cosmochim. Acta 198, 48–69. https://doi.org/10.1016/j.gca.2016.11.004.
Ruiz, J.M., Guillén, J.E., Ramos-Segura, A., Otero, M.M., 2015a. Atlas de las praderas marinas de España. Obs. Medioambient. 15, 681.
Ruiz, J.M., Guillén, J.E., Ramos-Segura, A., Otero, M.M., Guillén, E., Ramos Segura, A., Otero, M.M., 2015. Atlas de las praderas marinas de España., Observación medioambiental. IEO/IEL/UICN, Murcia-Alicante-Málaga.
Schoonen, M.A.A., 2004. Mechanisms of Sedimentary Pyrite Formation. https://doi.org/10.1130/0-8137-2379-5.117.
Shimmield, T.M., Black, K.D., Howe, J.A., Hughes, D.J., Sherwin, T., 2010. Independent Evaluation of Deep-Sea Mine Tailings Placement (DSTP) in PNG - Final Report.
Simonelli, L., Marini, C., Olszewski, W., Ávila Pérez, M., Ramanan, N., Guilera, G., Cuartero, V., Klementiev, K., 2016. CLAESS: the hard X-ray absorption beamline of the ALBA CELLS synchrotron. Cogent Phys. 3, 1–10. https://doi.org/10.1080/23311940.2016.1231987.
Simpson, S.L., Spadaro, D.A., 2016. Bioavailability and chronic toxicity of metal sulfide minerals to benthic marine invertebrates: implications for Deep Sea exploration, mining and tailings disposal. Environ. Sci. Technol. 50, 4061–4070. https://doi.org/10.1021/acs.est.6b00203.
Smedley, P., Kinniburgh, D., 2002. A review of the source, behaviour and distribution of arsenic in natural waters. Appl. Geochem. 17, 517–568. https://doi.org/10.1016/S0883-2927(02)00018-5.
Smith, P.G., Koch, I., Gordon, R.A., Mandoli, D.F., Chapman, B.D., Reimer, K.J., 2005. X-ray absorption near-edge structure analysis of arsenic species for application to biological environmental samples. Environ. Sci. Technol. 39, 248–254. https://doi.org/10.1021/es049358b.
Solomon, D., Lehmann, J., Zarruk, K.K., Dathe, J., Kinyangi, J., Liang, B., Machado, S., 2011. Speciation and long- and short-term molecular-level dynamics of soil organic sulfur studied by X-ray absorption near-edge structure spectroscopy. J. Environ. Qual. 40, 704–718. https://doi.org/10.2134/jeq2010.0061.
Sun, J., Hong, Y., Guo, J., Yang, J., Huang, D., Lin, Z., Jiang, F., 2019. Arsenite removal without thioarsenite formation in a sulfidogenic system driven by sulfur reducing bacteria under acidic conditions. Water Res. 151, 362–370. https://doi.org/10.1016/j.watres.2018.12.027.
Vairavamurthy, A., Zhou, W., Eglinton, T., Manowitz, B., 1994. Sulfonates: a novel class of organic sulfur compounds in marine sediments. Geochim. Cosmochim. Acta 58, 4681–4687. https://doi.org/10.1016/0016-7037(94)90200-3.
van der Walt, S., Colbert, S.C., Varoquaux, G., 2011. The NumPy Array: a structure for efficient numerical computation. Comput. Sci. Eng. 13, 22–30. https://doi.org/10.1109/MCSE.2011.37.
Van Dover, C.L., 2011. Tighten regulations on deep-sea mining. Nature https://doi.org/10.1038/470031a.
Virtanen, P., Gommers, R., Oliphant, T.E., Haberland, M., Reddy, T., Cournapeau, D., Burovski, E., Peterson, P., Weckesser, W., Bright, J., van der Walt, S.J., Brett, M., Wilson, J., Millman, K.J., Mayorov, N., Nelson, A.R.J., Jones, E., Kern, R., Larson, E., Carey, C.J., Polat, İ., Feng, Y., Moore, E.W., VanderPlas, J., Laxalde, D., Perktold, J., Cimrman, R., Henriksen, I., Quintero, E.A., Harris, C.R., Archibald, A.M., Ribeiro, A.H.,

Pedregosa, F., van Mulbregt, P., Vijaykumar, A., Bardelli, A.Pietro, Rothberg, A., Hilboll, A., Kloeckner, A., Scopatz, A., Lee, A., Rokem, A., Woods, C.N., Fulton, C., Masson, C., Häggström, C., Fitzgerald, C., Nicholson, D.A., Hagen, D.R., Pasechnik, D.V., Olivetti, E., Martin, E., Wieser, E., Silva, F., Lenders, F., Wilhelm, F., Young, G., Price, G.A., Ingold, G.-L., Allen, G.E., Lee, G.R., Audren, H., Probst, I., Dietrich, J.P., Silterra, J., Webber, J.T., Slavič, J., Nothman, J., Buchner, J., Kulick, J., Schönberger, J.L., de Miranda Cardoso, J.V., Reimer, J., Harrington, J., Rodríguez, J.L.C., Nunez-Iglesias, J., Kuczynski, J., Tritz, K., Thoma, M., Newville, M., Kümmerer, M., Bolingbroke, M., Tartre, M., Pak, M., Smith, N.J., Nowaczyk, N., Shebanov, N., Pavlyk, O., Brodtkorb, P.A., Lee, P., McGibbon, R.T., Feldbauer, R., Lewis, S., Tygier, S., Sievert, S., Vigna, S., Peterson, S., More, S., Pudlik, T., Oshima, T., Pingel, T.J., Robitaille, T.P., Spura, T., Jones, T.R., Cera, T., Leslie, T., Zito, T., Krauss, T., Upadhyay, U., Halchenko, Y.O., Vázquez-Baeza, Y., 2020. SciPy 1.0: fundamental algorithms for scientific computing in Python. Nat. Methods 17, 261–272. https://doi.org/10.1038/s41592-019-0686-2.

Vogt, C., 2013. International Assessment of Marine and Riverine Disposal of Mine Tailings: Final Report Adopted by the International Maritime Organization, London Convention/Protocol.

Walder, I., 2015. Sub-sea Tailings Deposition Evaluation Guideline. https://doi.org/10.13140/RG.2.1.4959.5366.

Wang, Y., Jiao, J.J., Zhu, S., Li, Y., 2013. Arsenic K-edge X-ray absorption near-edge spectroscopy to determine oxidation states of arsenic of a coastal aquifer-aquitard system. Environ. Pollut. 179, 160–166. https://doi.org/10.1016/j.envpol.2013.04.005.

Wang, Y., Rong, Z., Tang, X., Cao, S., 2019. Design of Scorodite@Fe3O4 core-shell materials and the Fe3O4 shell prevents leaching of arsenic from scorodite in neutral and alkaline environments. Coatings 9, 523. https://doi.org/10.3390/coatings9080523.

Wang, H.Y., Byrne, J.M., Perez, J.P.H., Thomas, A.N., Göttlicher, J., Höfer, H.E., Mayanna, S., Kontny, A., Kappler, A., Guo, H.M., Benning, L.G., Norra, S., 2020. Arsenic sequestration in pyrite and greigite in the buried peat of As-contaminated aquifers. Geochim. Cosmochim. Acta 284, 107–119. https://doi.org/10.1016/j.gca.2020.06.021.

Wilke, M., Farges, F., Petit, P.E., Brown, G.E., Martin, F., 2001. Oxidation state and coordination of Fe in minerals: an Fe K-XANES spectroscopic study. Am. Mineral. 86, 714–730. https://doi.org/10.2138/am-2001-5-612.

Xia, K., Weesner, F., Bleam, W.F., Helmke, P.A., Bloom, P.R., Skyllberg, U.L., 1998. XANES studies of oxidation states of sulfur in aquatic and soil humic substances. Soil Sci. Soc. Am. J. 62, 1240–1246. https://doi.org/10.2136/sssaj1998.03615995006200050014x.